Mathematical Analysis of SAR Imaging through a Turbulent Ionosphere

M. Gilman[1] and S. Tsynkov[1,2,a)]

[1]*Department of Mathematics, North Carolina State University, Box 8205, Raleigh, NC 27695, USA*
[2]*Moscow Institute of Physics and Technology, Dolgoprudny 141700, Russia*

[a)]Corresponding author: tsynkov@math.ncsu.edu

Abstract. Synthetic aperture radar (SAR) imaging though the Earth ionosphere is subject to distortions due to ionospheric turbulence. We consider the limiting cases of small-scale and large-scale turbulence and characterize the distortions in terms of image blurring and azimuthal shift. It is shown that in the large-scale case, a high level of eikonal fluctuations can coexist with the low degree of image distortions, and that blurring becomes significant at much higher levels of fluctuations than the shift. In the small-scale case, a low level of eikonal fluctuations is a precondition for imaging, while the magnitude of distortions depends on the ratio between the eikonal correlation radius and the length of the synthetic aperture.

1 INTRODUCTION

Synthetic aperture radar (SAR) is an imaging technology where electromagnetic pulses probe the target from several directions and special processing is applied to the scattered signals to achieve resolution. The signal processing procedure is sensitive to the velocity of signal propagation. When the antenna is mounted on a satellite orbiting the Earth, the signals travel through the ionosphere where the propagation speed varies. It depends on the characteristics of the ionospheric plasma and is affected by a number of factors, in particular, the plasma turbulence. For the analysis of ionospheric turbulence one commonly employs the statistical approach, which, in turn, calls for a statistical treatment of image distortions. Yet the case where the size of the synthetic aperture is much smaller than the correlation radius of turbulent fluctuations appears very close to that of the propagation through a deterministic plasma. In this case, the physical interpretation of the results obtained in the statistical framework is not straightforward.

We begin with an abridged and simplified exposition of standard SAR, *i.e.*, the case of unobstructed propagation of the signals, see Section 2. In Section 3, we discuss SAR imaging through a deterministic ionosphere. Imaging through a turbulent ionosphere is analyzed in Section 4. We first recall the small-scale case that we studied previously [1, Chapter 4]. In this case, a statistical approach readily applies. The central new contribution of the current paper is the analysis of the large-scale case in Section 4.4. First, we re-evaluate some earlier results and draw the necessary parallels to the deterministic setup of Section 3. In doing so, we still remain in the statistical framework that provides an adequate description of the plasma turbulence. Then, it turns out that while the small-scale case is conveniently described by the statistics of phases of the propagating signals, the large-scale case is easier to analyze using the statistics of the coefficients of a polynomial approximation to the signal phase as a function of the azimuthal coordinate. We find that the distortions in the large-scale case may be described in terms of image blurring and azimuthal shift. The former becomes essential at much larger levels of turbulent fluctuations than the latter. Additionally, we verify that the large-scale case tolerates much higher levels of turbulence than the small-scale case.

In this paper, we employ geometrical optics for the analysis of signal propagation, assume that the deterministic ionosphere is vertically homogeneous, and characterize the effect of ionospheric turbulence in terms of the intensity and correlation radius of eikonal fluctuations. While this approximate model proves sufficient for the current study, we refer the reader to our recent book [1] for a more detailed treatment of the background material and further references.

Application of Mathematics in Technical and Natural Sciences
AIP Conf. Proc. 1895, 020003-1–020003-23; https://doi.org/10.1063/1.5007357
Published by AIP Publishing. 978-0-7354-1579-9/$30.00

2 STANDARD SAR

This section introduces the main concepts and geometry of SAR imaging, as well as image processing formulation and characteristics of image quality. A more detailed presentation can be found in [1, Chapter 2] and references therein.

2.1 Signal Processing

Synthetic aperture radar (SAR) technology is realized via emitting electromagnetic signals of certain waveform and processing the received signals that are scattered about the target. A typical emitted signal is a frequency-modulated pulse, or chirp, with the central carrier frequency ω_0:

$$P(t) = A(t)e^{-i\omega_0 t}, \quad \text{where} \quad A(t) = \chi_\tau(t)e^{-i\alpha t^2} \tag{1}$$

and χ_τ is the indicator function:

$$\chi_\tau(t) = \begin{cases} 1, & t \in [-\tau/2, \tau/2], \\ 0, & \text{otherwise.} \end{cases} \tag{2}$$

In formula (1), $\alpha = \frac{B}{2\tau}$ is the chirp rate, $\frac{B}{2\pi}$ is called the bandwidth of the chirp (we consider $B > 0$), and τ is its duration. The chirp can be approximately thought of as a signal whose instantaneous frequency varies in time according to

$$\omega(t) \stackrel{\text{def}}{=} \frac{d}{dt}(\omega_0 t + \alpha t^2) = \omega_0 + 2\alpha t = \omega_0 + \frac{B}{\tau}t, \tag{3}$$

where according to (2), the interval of variation is $\omega_0 - B/2 \leqslant \omega \leqslant \omega_0 + B/2$. The time-bandwidth product of the chirp, $\frac{B\tau}{2\pi}$, also known as its compression ratio, is assumed large: $B\tau \gg 1$; this allows one to achieve spatial resolution much better than $c\tau$. Typically, narrow-band pulses are used, so $B \ll \omega_0$.

The scalar incident field in 3D emitted from the point $\boldsymbol{x}$ and governed by the d'Alembert equation is given by the standard retarded potential:

$$u^{(0)}(t, \boldsymbol{z}) = \frac{1}{4\pi}\frac{P(t - |\boldsymbol{z} - \boldsymbol{x}|/c)}{|\boldsymbol{z} - \boldsymbol{x}|}, \tag{4}$$

where c is the speed of light. The scattered field under the first Born approximation (also called the single-scattering approximation) received at the same point $\boldsymbol{x}$ is

$$u^{(1)}(t, \boldsymbol{x}) \approx \int \nu(\boldsymbol{z}) P\left(t - 2|\boldsymbol{z} - \boldsymbol{x}|/c\right) d\boldsymbol{z}, \tag{5}$$

where $\nu(\boldsymbol{z})$ is the target reflectivity function that also incorporates several other factors such as the propagation attenuation, antenna radiation pattern, *etc.*, that are assumed constant for the entire image. The integration limits in (5) are finite because $P(\,\cdot\,)$ contains the indicator function (2).

To solve the inverse scattering problem for SAR means to obtain $\nu(\boldsymbol{z})$ from the known $u^{(1)}(t, \boldsymbol{x})$. In other words, one needs to invert the integral operator that acts on $\nu(\boldsymbol{z})$ on the right-hand side of (5). The approximate inversion, which is also called the SAR signal processing, is done in two stages. First, the received signal $u^{(1)}(t, \boldsymbol{x})$ given by (5) is multiplied by the function $\overline{P(t - 2|\boldsymbol{y} - \boldsymbol{x}|/c)}$, where the overbar denotes complex conjugate and $\boldsymbol{y}$ represents the image coordinate, and integrated with respect to t. This yields the so-called single-pulse image:

$$I_x(\boldsymbol{y}) = \int \overline{P(t - 2R_y/c)} u^{(1)}(t, \boldsymbol{x})\, dt = \int d\boldsymbol{z}\, \nu(\boldsymbol{z}) \underbrace{\int dt\, \overline{P(t - 2R_y/c)} P(t - 2R_z/c)}_{W_x(\boldsymbol{y}, \boldsymbol{z})} = \int W_x(\boldsymbol{y}, \boldsymbol{z}) \nu(\boldsymbol{z})\, d\boldsymbol{z}, \tag{6}$$

where

$$R_y \stackrel{\text{def}}{=} |\boldsymbol{y} - \boldsymbol{x}| \quad \text{and} \quad R_z \stackrel{\text{def}}{=} |\boldsymbol{z} - \boldsymbol{x}|.$$

In doing so, we assume that both $\boldsymbol{y}$ and $\boldsymbol{z}$ are within the footprint of the antenna beam located at $\boldsymbol{x}$, see Figure 1. The procedure described by (6) is called the matched filtering because for $R_y = R_z$, the integrand in the expression that yields $W_x(\boldsymbol{y}, \boldsymbol{z})$ is constant.

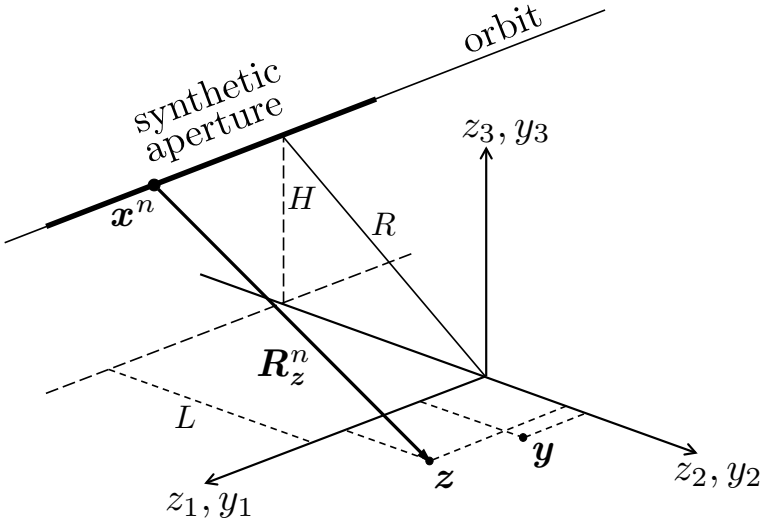

FIGURE 1. Schematic for the monostatic broadside stripmap SAR imaging. H is the orbit altitude, L is the distance (range) from the ground track to the target, R is the slant range

At the final stage of the inversion, we take a sequence of radar pulses emitted from the equally spaced positions $\boldsymbol{x}^n = (x_1^n, -L, H)$ that form the synthetic array as the antenna moves along the linear flight track (orbit), see Figure 1. For stripmap imaging, we assume $x_1^n = (y_1 + z_1)/2 + nL_{\rm SA}/N$ (see [1, Section 2.4.2] for more detail), where $-N/2 \leqslant n \leqslant N/2$, $N \gg 1$ is the number of pulses, and $L_{\rm SA}$ is the length of the synthetic array or, equivalently, synthetic aperture. SAR systems are specifically designed to operate in the near-field zone of the synthetic array. Hence, the Fresnel number computed for the aperture of size $L_{\rm SA}$ should be large: $\mathfrak{F} = L_{\rm SA}^2/(R\lambda_0) \gg 1$, where $\lambda_0 = 2\pi c/\omega_0$ is the carrier wavelength. Repeating the procedure described by (5)–(6) for each $\boldsymbol{x}^n$ and adding together the resulting single-pulse images, we arrive at

$$
\begin{aligned}
I(\boldsymbol{y}) = \sum_n I_{\boldsymbol{x}^n}(\boldsymbol{y}) &= \sum_n \int \overline{P(t - 2R_{\boldsymbol{y}}^n/c)} u^{(1)}(t, \boldsymbol{x}^n)\, dt \\
&= \int d\boldsymbol{z}\, \nu(\boldsymbol{z}) \underbrace{\sum_n \int dt\, \overline{P(t - 2R_{\boldsymbol{y}}^n/c)} P(t - 2R_{\boldsymbol{z}}^n/c)}_{W(\boldsymbol{y},\boldsymbol{z})} = \int W(\boldsymbol{y}, \boldsymbol{z}) \nu(\boldsymbol{z})\, d\boldsymbol{z}.
\end{aligned} \tag{7}
$$

In formula (7), $R_{\boldsymbol{y}}^n \stackrel{\rm def}{=} |\boldsymbol{y} - \boldsymbol{x}^n|$ and $R_{\boldsymbol{z}}^n \stackrel{\rm def}{=} |\boldsymbol{z} - \boldsymbol{x}^n|$. Similarly to (6), we assume that all points $\boldsymbol{y}$ and $\boldsymbol{z}$ are within the intersection of the antenna beam footprints for the set of locations $\{\boldsymbol{x}^n\}$, see Figure 1.

2.2 Generalized Ambiguity Function and Resolution

For the points $\boldsymbol{y} = (y_1, y_2, 0)$ and $\boldsymbol{z} = (z_1, z_2, 0)$ in the target area, we assume that the following condition is satisfied: $|\boldsymbol{y}|, |\boldsymbol{z}| \ll L_{\rm SA} \ll R$, see Figure 1. Then, from the Pythagorean theorem, we have:

$$
T^n = \frac{R_{\boldsymbol{y}}^n - R_{\boldsymbol{z}}^n}{c} \approx \frac{1}{c}\Big(\frac{L}{R}(y_2 - z_2) - \frac{L_{\rm SA}}{NR}(y_1 - z_1)n\Big). \tag{8}
$$

Carrying out the integration in (6) under the assumptions that $B\tau \gg 1$ and $|y_2 - z_2| \ll c\tau$, we can express the single-pulse point spread functions (PSFs) $W_{\boldsymbol{x}^n}$ as

$$
W_{\boldsymbol{x}^n}(\boldsymbol{y}, \boldsymbol{z}) = e^{-2i\omega_0 T^n} \int\limits_{-\tau/2+|T^n|}^{\tau/2-|T^n|} e^{-4i\alpha T^n t} dt \approx e^{-2i\omega_0 T^n} \tau\, \mathrm{sinc}(BT^n), \tag{9}
$$

where $\operatorname{sinc}\xi \stackrel{\text{def}}{=} \sin\xi/\xi$. Then, the multi-pulse PSF $W(\boldsymbol{y},\boldsymbol{z})$ of (7), also called the generalized ambiguity function (GAF), becomes:

$$W(\boldsymbol{y},\boldsymbol{z}) = \sum_n W_{\boldsymbol{x}^n}(\boldsymbol{y},\boldsymbol{z}) = \tau \sum_n e^{-2i\omega_0 T^n} \operatorname{sinc}(BT^n). \tag{10}$$

As $B \ll \omega_0$, formula (10) can be simplified by disregarding the dependence of T^n on n under the sinc function (but not in the exponent). Performing the summation similarly to the integration in (9) under the assumption that $\mathfrak{F} \gg 1$, we obtain a factorized approximation to $W(\boldsymbol{y},\boldsymbol{z})$:

$$W_{(\mathrm{R}\Sigma)}(\boldsymbol{y},\boldsymbol{z}) = \tau \operatorname{sinc}(BT^0) \sum_n e^{-2i\omega_0 T^n} \approx \underbrace{\tau \operatorname{sinc}(BT^0)}_{W_{\mathrm{R}}(\boldsymbol{y},\boldsymbol{z})} \cdot \underbrace{Ne^{-2i\omega_0 T^0} \operatorname{sinc}\left(\frac{\omega_0 L_{\mathrm{SA}}}{cR}(y_1 - z_1)\right)}_{W_{\Sigma}(\boldsymbol{y},\boldsymbol{z})}, \tag{11}$$

where $T^0 = L(y_2 - z_2)/(cR)$, see (8).

Spatial resolution is one of the most important characteristics of the image. The convolution representation of $I(\boldsymbol{y})$ given by (7) allows us to think of the GAF $W(\boldsymbol{y},\boldsymbol{z}_0)$ as of the image of a point scatterer $\nu(\boldsymbol{z}) = \delta(\boldsymbol{z} - \boldsymbol{z}_0)$. Hence, we will define the resolution sizes in range and azimuth as half-width of the main lobe of the sinc function in W_{R} and W_{Σ}, respectively. From (11), we obtain:

$$\Delta_{\mathrm{R}} = \frac{\pi c}{B}\frac{R}{L}, \quad \Delta_{\mathrm{A}} = \frac{\pi R c}{\omega_0 L_{\mathrm{SA}}}. \tag{12}$$

As we have mentioned earlier, $\Delta_{\mathrm{R}} \ll c\tau$ due to $B\tau \gg 1$. Similarly, $\Delta_{\mathrm{A}} \ll L_{\mathrm{SA}}$ because $\mathfrak{F} \gg 1$, see [1, Section 2.6].

2.3 Factorization Error

As indicated previously, the factorized expression $W_{(\mathrm{R}\Sigma)}$ of (11) is an approximation to the actual GAF given by (10). The difference between the two can be expressed as

$$W - W_{(\mathrm{R}\Sigma)} = \tau \sum_n e^{-2i\omega_0 T^n} [\operatorname{sinc}(BT^n) - \operatorname{sinc}(BT^0)]. \tag{13}$$

Obviously, this difference is due to the dependence of T^n on n, see (8). As $L_{\mathrm{SA}}/R \ll 1$, we can use the expansion

$$\operatorname{sinc}(BT^n) \approx \operatorname{sinc}(BT^0) - \operatorname{sinc}'(BT^0) \cdot \frac{B}{c}\frac{L_{\mathrm{SA}}}{NR}(y_1 - z_1)n. \tag{14}$$

Then, using $\sum_n ne^{in\psi} \approx \frac{N^2}{2i} \operatorname{sinc}' \frac{N\psi}{2}$ for $|\psi| \ll 1$ and $N \gg 1$, we perform the summation in (13) and obtain:

$$W - W_{(\mathrm{R}\Sigma)} \approx \frac{i}{2}\frac{B}{\omega_0} N\tau \frac{\pi(y_1 - z_1)}{\Delta_{\mathrm{A}}} \operatorname{sinc}'(BT^0) \operatorname{sinc}' \frac{\pi(y_1 - z_1)}{\Delta_{\mathrm{A}}}. \tag{15}$$

Limiting the consideration to the main azimuthal lobe, *i.e.*, $\pi|y_1 - z_1| \leqslant \Delta_{\mathrm{A}}$, and taking into account the properties of the sinc function, we get:

$$\frac{\max|W - W_{(\mathrm{R}\Sigma)}|}{\max|W_{(\mathrm{R}\Sigma)}|} \lesssim \frac{\pi}{8}\frac{B}{\omega_0}. \tag{16}$$

The left-hand side of (16) is called the factorization error and may be given the following interpretation. The main lobe of $W_{(\mathrm{R}\Sigma)}$ is clearly outlined, both in range and in azimuth, by the leading zeros of the corresponding sinc functions. Yet expression (15) does not vanish at the edges of the main lobe of $W_{(\mathrm{R}\Sigma)}$. Hence, the main lobe of the true GAF $W = W_{(\mathrm{R}\Sigma)} + (W - W_{(\mathrm{R}\Sigma)})$ is not so well defined. In other words, the image of a point scatterer will have a decreased contrast due to smearing of the edges of the main lobe. Expression (16) quantifies this effect. For a narrow-band interrogating pulse, $B \ll \omega_0$, the degree of smearing is small.

3 SAR IMAGING THROUGH A DETERMINISTIC IONOSPHERE

In this section, we analyze how the dispersion of radio waves in the ionospheric plasma affects the SAR imaging as presented in Section 2. The ionosphere is considered deterministic. For conciseness, we are also assuming that it is vertically homogeneous and may vary only horizontally in the azimuthal direction. This is consistent with our subsequent finding that the ionospheric turbulence mainly affects the SAR performance in azimuth (see Section 4). A more detailed analysis of the deterministic case can be found, *e.g.*, in [1, Chapter 3] and the references therein.

3.1 Modification of the Signal and GAF Due to the Dispersion in Plasma

The dispersion of electromagnetic waves in plasma is due to the presence of free charged particles, most importantly — electrons. The electrons move in the field of the propagating electromagnetic wave, and as they move, they also emit radiation. Thus, the impinging field gets modified. For transverse monochromatic electromagnetic waves with the frequency ω, the dispersion relation reads:

$$\omega^2 = \omega_{\mathrm{pe}}^2 + c^2k^2, \quad \text{where} \quad \omega_{\mathrm{pe}}^2 = \frac{4\pi e^2 N_{\mathrm{e}}}{m_{\mathrm{e}}}, \quad k = \frac{2\pi}{\lambda}. \tag{17}$$

This is notably different from the relation $\omega = kc$ that characterizes the propagation in vacuum. In formula (17), $-e$, N_{e}, and m_{e} are the electron charge, number density, and mass, respectively, ω_{pe} is the electron plasma (Langmuir) frequency, and k is the wavenumber. Accordingly, the phase and group velocity of high-frequency electromagnetic waves that propagate in the plasma characterized by (17) differ from the speed of light:

$$v_{\mathrm{ph}} = \frac{\omega}{k} = c\Big(1 + \frac{\omega_{\mathrm{pe}}^2}{c^2k^2}\Big)^{\frac{1}{2}} \approx c\Big(1 + \frac{\omega_{\mathrm{pe}}^2}{2\omega^2}\Big), \tag{18a}$$

$$v_{\mathrm{gr}} = \frac{d\omega}{dk} = c\Big(1 + \frac{\omega_{\mathrm{pe}}^2}{c^2k^2}\Big)^{-\frac{1}{2}} \approx c\Big(1 - \frac{\omega_{\mathrm{pe}}^2}{2\omega^2}\Big). \tag{18b}$$

In (18), we assumed that $\omega \gg \omega_{\mathrm{pe}}$, which is typical for the parameters of radar systems and the Earth's ionosphere. Hence, different frequencies that compose the chirp, see (3), will propagate with different velocities. This leads to a modification of the chirp waveform. It can be shown that instead of (4), the propagation of a chirp is described by

$$u^{(0)}(t, \boldsymbol{z}) = \frac{1}{4\pi|\boldsymbol{z} - \boldsymbol{x}|} A'(t - |\boldsymbol{z} - \boldsymbol{x}|/v_{\mathrm{gr}}(\omega_0)) e^{-i\omega_0(t - |\boldsymbol{z}-\boldsymbol{x}|/v_{\mathrm{ph}}(\omega_0))}, \tag{19}$$

where

$$A'(t) = \chi_{\tau'}(t)\sqrt{\frac{1}{1 - \delta\tau/\tau}} e^{-i\alpha' t^2}, \quad \tau' = \tau - \delta\tau, \quad \alpha' = \alpha\Big(1 - \frac{\delta\tau}{\tau}\Big)^{-1}, \quad \delta\tau = \frac{B}{\omega_0}\frac{|\boldsymbol{z} - \boldsymbol{x}|}{c}\frac{\omega_{\mathrm{pe}}^2}{\omega_0^2}. \tag{20}$$

Typically, $|\delta\tau/\tau|$ is small, on the order of 10^{-3} or less. Note that the propagation in a medium that is inhomogeneous along the ray path (in particular, a vertically inhomogeneous ionosphere) can be incorporated into the formulation (19)–(20) by introducing an effective plasma frequency. This frequency is calculated using a parameter called the total electron content (TEC), which is an integral of the electron number density along the ray path, see [1, Section 3.3].

If the standard SAR signal processing (6)–(7) is applied to the received signals described by (19)–(20), then the image will still be given by a convolution integral:

$$I(\boldsymbol{y}) = \int W'(\boldsymbol{y}, \boldsymbol{z}) \nu(\boldsymbol{z})\, d\boldsymbol{z}, \quad \text{where} \quad W'(\boldsymbol{y}, \boldsymbol{z}) \approx \sum_n e^{-2i\omega_0 T_{\mathrm{ph}}^n} \int_{-\tau/2}^{\tau/2} e^{2i(\alpha - \alpha')t^2} e^{-4i\alpha T_{\mathrm{gr}}^n t} dt, \quad T_{\mathrm{gr,ph}}^n = \frac{R_y^n}{c} - \frac{R_z^n}{v_{\mathrm{gr,ph}}}. \tag{21}$$

The velocities $v_{\mathrm{gr,ph}}$ in (21) are evaluated using (18) for $\omega = \omega_0$. Certain inessential effects, such as a minor variation of the signal amplitude, as well as of the integration limits, due to $\delta\tau$ of (20), have been disregarded in (21).

3.2 Image Distortions Due to Dispersive Propagation

We will analyze the distortions of images built with the help of $W'(\boldsymbol{y}, \boldsymbol{z})$ given by (21).

3.2.1 *Effects due to dispersive propagation through a homogeneous plasma*

This class of effects can be described using the factorized representation:

$$W'(\boldsymbol{y},\boldsymbol{z}) \approx W'_{\mathrm{R}}(\boldsymbol{y},\boldsymbol{z}) \cdot W'_{\Sigma}(\boldsymbol{y},\boldsymbol{z}), \quad \text{where} \quad W'_{\mathrm{R}}(\boldsymbol{y},\boldsymbol{z}) = \int\limits_{-\tau/2}^{\tau/2} e^{2i(\alpha-\alpha')t^2} e^{-4i\alpha' T^0_{\mathrm{gr}} t} dt, \quad W'_{\mathrm{A}}(\boldsymbol{y},\boldsymbol{z}) = \sum_n e^{-2i\omega_0 T^n_{\mathrm{ph}}}. \tag{22}$$

Resolution and shift in range. Substituting (18b) into the last formula of (21), we can represent T^0_{gr} as

$$T^0_{\mathrm{gr}} \approx \frac{R^0_y - R^0_z}{c} - \frac{R^0_z}{c}\frac{\omega^2_{\mathrm{pe}}}{2\omega_0^2}. \tag{23}$$

Neglecting for the moment the quadratic phase term in the expression for W'_{R} in (22), we obtain: $W'_{\mathrm{R}} \approx \tau\,\mathrm{sinc}(BT^0_{\mathrm{gr}})$. This expression peaks at $T^0_{\mathrm{gr}} = 0$, that is, when

$$(y_2 - z_2)\frac{L}{R} = R^0_z \frac{\omega^2_{\mathrm{pe}}}{2\omega_0^2} \approx R\frac{\omega^2_{\mathrm{pe}}}{2\omega_0^2}. \tag{24}$$

Thus, the image of a point scatterer appears shifted from its true position in range. The direction of the shift is away from the antenna. For a satellite-based system, this shift may reach hundreds of meters.

At the same time, the factor at y_2 in the exponent of $e^{-4i\alpha' T^0_{\mathrm{gr}} t} = e^{-4i\alpha' L(y_2-z_2)t/(Rc)}$ has changed little compared to unobstructed propagation, see (9). Hence, the change in the resolution size as defined in Section 2.2 is small.

Quadratic phase error in range. Consider a more general form of the integral in the expression for W'_{R} in (22):

$$\mathcal{W}(\kappa,\phi) = \int\limits_{-1/2}^{1/2} e^{-2i\kappa s} e^{4i\phi s^2} ds. \tag{25}$$

The variable ϕ in (25) is called the quadratic phase error (QPE). When $\phi = 0$, the integral in (25) reduces to that with a linear phase (see (9)), and $\mathcal{W}(\kappa, 0) = \mathrm{sinc}\,\kappa$. When $\phi \neq 0$, the integral can be evaluated using the erf functions. Its asymptotics as $\phi \to 0$ can be calculated with the help of a Taylor expansion for $e^{4i\phi s^2}$. In particular, we are interested in the expressions for $\kappa = 0$ and $\kappa = \pi$:

$$\mathcal{W}(0,\phi) \approx 1 + \frac{1}{3}i\phi - \frac{1}{10}\phi^2 \Longrightarrow |\mathcal{W}(0,\phi)| \approx 1 - \frac{2}{45}\phi^2, \quad \mathcal{W}(\pi,\phi) \approx -\frac{2}{\pi^2}i\phi. \tag{26}$$

For the imaging operator $\nu(z) \mapsto I(y)$, see (7), the QPE ϕ contributes to the filter mismatch. Specifically, for W'_{R} given by (22), the quantity $|\mathcal{W}(0,\phi)|$ characterizes the relative decrease of the peak height of $W'_{\mathrm{R}}(y_2 - z_2)$ due to the QPE, while $|\mathcal{W}(\pi,\phi)|$ describes the smearing of the edge of the main range lobe in the range direction as a function of the QPE. Taking into account that $\mathcal{W}(\pi, 0) = 1$ and $\mathcal{W}(\pi, 0) = 0$, we see that the distortions of the image of a point scatterer can be quantified in terms of either the decrease of the peak amplitude, *i.e.*, $1 - |\mathcal{W}(0,\phi)|$, or the value at the edge of the main lobe: $|\mathcal{W}(\pi,\phi)|$. In particular, from (22) and (25), we have:

$$W'_{\mathrm{R}} = \tau\mathcal{W}\Big(\pi\frac{y_2 - z_2}{\Delta_{\mathrm{R}}}, \phi_{\mathrm{R}}\Big), \quad \text{where} \quad \phi_{\mathrm{R}} = (\alpha - \alpha')\frac{\tau^2}{2} \approx -\frac{1}{4}\frac{B}{\omega_0}\frac{BR}{c}\frac{\omega^2_{\mathrm{pe}}}{\omega_0^2}.$$

Resolution and quadratic phase error in azimuth. For T^n_{ph}, we can write:

$$T^n_{\mathrm{ph}} \approx \underbrace{-\frac{1}{2}\Big(\frac{1}{c} + \frac{1}{v_{\mathrm{ph}}}\Big)(y_1 - z_1)n\frac{L_{\mathrm{SA}}}{NR}}_{\approx T^n} + \frac{1}{2R}\Big(\frac{1}{c} - \frac{1}{v_{\mathrm{ph}}}\Big)\Big(n\frac{L_{\mathrm{SA}}}{N}\Big)^2 + T_{\mathrm{const}}\,. \tag{27}$$

Note that the leading term due to $\omega_{\rm pe}^2$ that is similar to the one that yields the shift of $W'_{\rm R}$, see (23)–(24), has been included here into the term $T_{\rm const}$ that is independent on n. Indeed, as $T_{\rm ph}^n$ enters the expression for $W'_{\rm A}$ in the exponents under the sum, see (22), a term that does not depend on n results in a phase shift of $W'_{\rm A}$ (and, as the result, of the entire image), which is often treated as not a distortion. Similarly to the case of $W'_{\rm R}$, the term linear in n appears essentially the same as that for the unobstructed propagation, so we can write:

$$W'_{\rm A} \approx e^{-2i\omega_0 T_{\rm const}} \sum_n e^{-2i\omega_0 T^n} e^{-i\frac{\omega_0}{c}\frac{L_{\rm SA}^2}{R}\frac{\omega_{\rm pe}^2}{2\omega_0^2}n^2}.$$

Hence, the azimuthal resolution is practically unaffected. The effects due to the QPE can be evaluated once the summation over n is replaced with integration with the limits of $\pm N/2$. This yields:

$$W'_{\rm A} = N\mathcal{W}\Big(\pi\frac{y_1 - z_1}{\Delta_{\rm A}}, \phi_{\rm A}\Big), \quad \text{where} \quad \phi_{\rm A} = \frac{1}{8}\frac{\omega_0}{c}\frac{L_{\rm SA}^2}{R}\frac{\omega_{\rm pe}^2}{\omega_0^2} \tag{28}$$

and $\mathcal{W}$ is introduced by formulae (25)–(26).

3.2.2 Effects due to large-scale azimuthal variation of plasma density

The simplest way to take into account the azimuthal variation of the ionosphere is to formally consider $\omega_{\rm pe}$ in (18) a smooth function of the antenna coordinate $x_1^n = nL_{\rm SA}/N$ (for a more accurate derivation, see [1, Section 3.9]). The following representation is convenient to use:

$$\omega_{\rm pe}^2(n) \approx \tilde{\omega}_{\rm pe}^2\Big(1 + \frac{L_{\rm SA}}{L_Q}\frac{n}{N} + \frac{L_{\rm SA}^2}{L_Q L_P}\frac{n^2}{N^2}\Big). \tag{29}$$

Formula (29) is basically the second order Taylor expansion of $\omega_{\rm pe}^2(n)$ about $n = 0$. The constant L_Q in (29) can be thought of as the scale of the linear part of variation of the electron number density in the ionosphere, while L_P is the scale of the linear part of variation of L_Q. The following effects are caused by the dependence $\omega_{\rm pe}^2 = \omega_{\rm pe}^2(n)$ given by (29).

Azimuthal shift and QPE. From formula (29), we obtain [cf. formula (27)]:

$$T_{\rm ph}^n \approx \frac{R}{c}\frac{\tilde{\omega}_{\rm pe}^2}{2\omega_0^2}\Big(\frac{L_{\rm SA}}{L_Q}\frac{n}{N} + \frac{L_{\rm SA}^2}{L_Q L_P}\frac{n^2}{N^2}\Big) - \frac{1}{2}\Big(\frac{1}{c} + \frac{1}{v_{\rm ph}}\Big)(y_1 - z_1)n\frac{L_{\rm SA}}{NR} + \frac{1}{2R}\Big(\frac{1}{c} - \frac{1}{v_{\rm ph}}\Big)\Big(n\frac{L_{\rm SA}}{N}\Big)^2 + T_{\rm const}\,. \tag{30}$$

Using the factorized representation (22), combining the linear terms with respect to n in (30) and dropping the quadratic terms, we see that the peak of $W'_{\rm A}$ corresponds to

$$y_1 - z_1 = \frac{R^2}{L_Q}\frac{\tilde{\omega}_{\rm pe}^2}{2\omega_0^2}. \tag{31}$$

Similarly to (24), this relation means that the image is shifted in azimuth by the value of the right-hand side of (31). Unlike in (24), the sign of the shift is determined by the sign of L_Q in (29).

In turn, combining the quadratic terms with respect to n in formula (30), we express the modified QPE as

$$\phi'_{\rm A} = \phi_{\rm A} + \phi_{\rm inhom}, \quad \text{where} \quad \phi_{\rm inhom} \stackrel{\rm def}{=} \frac{1}{4}\frac{\omega_0 R}{c}\frac{L_{\rm SA}^2}{L_Q L_P}\frac{\omega_{\rm pe}^2}{\omega_0^2}. \tag{32}$$

In (32), the baseline QPE, *i.e.*, $\phi_{\rm A}$, is computed by substituting $\tilde{\omega}_{\rm pe}^2$ of (29) instead of $\omega_{\rm pe}^2$ in (28). Depending on the sign of $L_Q L_P$, the term $\phi_{\rm inhom}$, which is due to the large-scale variation of the plasma electron frequency, may either amplify or reduce the effect of the baseline QPE.

Effect on factorization error. Retaining only the leading term due to L_Q in $T^n_{\rm gr}$, we obtain:

$$T^n_{\rm gr} \approx \frac{R^n_y - R^n_z}{c} - \frac{R}{c}\frac{\tilde\omega^2_{\rm pe}}{2\omega_0^2}\Big(1 + \frac{L_{\rm SA}}{L_Q}\frac{n}{N}\Big) \approx \frac{1}{c}\Big(\frac{L}{R}(y_2 - z_2) - \frac{L_{\rm SA}}{NR}(y_1 - z_1)n - R\frac{\tilde\omega^2_{\rm pe}}{2\omega_0^2}\Big(1 + \frac{L_{\rm SA}}{L_Q}\frac{n}{N}\Big)\Big), \tag{33}$$

see (8) and (23). Out of the two terms proportional to n on the right-hand side of (33), the first one can be recognized as the source of the factorization error in the case of unobstructed propagation, see (14). The same procedure can be applied to the second term linear in n. In doing so, the first term can be dropped provided that $\frac{R}{|L_Q|}\frac{\tilde\omega^2_{\rm pe}}{\omega_0^2}\frac{L_{\rm SA}}{\lambda_0} \gg 1$ (λ_0 is the carrier wavelength), *i.e.*, provided that the azimuthal gradient of $\omega^2_{\rm pe}$ in (29) is sufficiently large (see [1, Sections 3.7 and 3.9] for more detail). Then, we obtain a new formula for the factorization error:

$$\frac{|W' - W'_{(\mathrm{R}\Sigma)}|}{\max|W_{(\mathrm{R}\Sigma)}|} \approx \frac{\pi}{8}\frac{B}{\omega_0}\frac{R}{|L_Q|}\frac{\tilde\omega^2_{\rm pe}}{\omega_0^2}\frac{L_{\rm SA}}{\lambda_0}. \tag{34}$$

Under certain ionospheric conditions, this value can be an order of magnitude larger than that given by (16).

3.3 Matched Filter Corrected for the Ionosphere

In order to mitigate the ionospheric effects on SAR images, the speed of light in the standard filter $P(t, n, \boldsymbol{y}) = \overline{P(t - 2R^n_y/c)}$, see (7), should be replaced with the phase and group velocity that characterize the ionospheric propagation (19):

$$P'(t, n, \boldsymbol{y}) = \overline{A'(t - 2R^n_y/v_{\rm gr}(n))}e^{i\omega_0(t - 2R^n_y/v_{\rm ph}(n))}. \tag{35}$$

The velocities $v_{\rm gr,ph}$ in (35) should be calculated according to (18), taking into account the dependence of $\omega^2_{\rm pe}$ on n given by (29), if necessary. Construction of such a filter requires knowledge of the electron number density in (17). In the case of a large-scale azimuthal inhomogeneity, it also requires information about the scales in (29). Such information can be derived from the analysis of image distortions. It can also be obtained from ionospheric models and observations. Then, one can show (see [1, Chapter 3]) that the corrected filter essentially eliminates the distortions due to dispersive propagation, and the characteristics of the resulting image reduce to those described in Section 2.

4 SAR IMAGING THROUGH A TURBULENT IONOSPHERE

Statistical methods are commonly used in the context of propagation of waves through turbulent or random media, see, *e.g.*, [2–4]. In this section, we will demonstrate some of the techniques and caveats of the statistical approach to SAR imaging. Presentation of the material through Section 4.3.2 follows [1, Chapter 4].

4.1 Characterization of Turbulence for Use in SAR

Random component of electron number density. In order to describe the propagation of radar pulses through a turbulent ionosphere, we represent the electron number density $N_{\rm e}$ as the sum of two components — deterministic and stochastic:

$$N_{\rm e} = \langle N_{\rm e}\rangle + \mu(\boldsymbol{x}). \tag{36}$$

Hereafter, the angular brackets $\langle\,\cdot\,\rangle$ denote the expected value (*i.e.*, mean) of a given random variable. For the analysis in the this paper, we will assume that the deterministic part of a turbulent ionosphere, *i.e.*, the background, does not vary in space: $\langle N_{\rm e}\rangle = \mathrm{const}$. Accordingly, the function $\mu = \mu(\boldsymbol{x})$ in (36) that accounts for the turbulent fluctuations of the ionosphere will be considered a homogeneous and isotropic random field with zero mean, see [5, Chapter I]. (The case of a slowly varying $\langle N_{\rm e}\rangle$, where μ becomes a quasi-homogeneous random field, is discussed in [1, Chapter 4].)

With the electron number density given by (36), the expressions for the travel times between $\boldsymbol{x}$ and $\boldsymbol{z}$ become:

$$\mathfrak{T}_{\rm ph,gr}(\boldsymbol{x}, \boldsymbol{z}) = \frac{R_z}{c}\left\{1 \mp \frac{\bar\omega^2_{\rm pe}}{2\omega_0^2} \mp \frac{1}{2}\frac{4\pi e^2}{m_{\rm e}\omega_0^2}\frac{1}{R_z}\int_0^{R_z}\mu(\boldsymbol{x}(r))dr\right\}, \tag{37}$$

where $\bar{\omega}_{\mathrm{pe}}^2$ is defined by (17) via the deterministic part $\langle N_{\mathrm{e}} \rangle$ of the electron number density only. Formula (37) generalizes the previously used deterministic expressions $R_z / v_{\mathrm{ph,gr}}$. It assumes a straight signal trajectory between the points $\boldsymbol{x}$ and $\boldsymbol{z}$, which is an implication of the geometrical optics approximation. A justification of this assumption for the propagation through a turbulent ionosphere is given in [1, Appendix 4.B]

Formula (37) defines $\mathfrak{T}_{\mathrm{ph,gr}}(\boldsymbol{x}, \boldsymbol{z})$ as random functions of their arguments. However, the first two terms in the brackets on the right-hand side of (37) are deterministic and coincide with $R_z / \bar{v}_{\mathrm{ph,gr}}$, where $\bar{v}_{\mathrm{ph,gr}}$ are defined by (18) with $\bar{\omega}_{\mathrm{pe}}$ used as the plasma frequency. The remaining integral on the right-hand side of (37) is what accounts for the randomness of the propagation medium. It is responsible for filter mismatches and the resulting image distortions due to ionospheric turbulence. The effect of this term cannot be compensated for without having some specific information about the random field μ.

In order to quantify the random contributions into the phases of SAR signals as given by (37), let us introduce

$$\varphi = \varphi(\boldsymbol{x}, \boldsymbol{z}) \stackrel{\mathrm{def}}{=} \frac{4\pi e^2}{m_{\mathrm{e}} \omega_0^2} \int_0^{R_z} \mu(\boldsymbol{x}(r))\, dr. \tag{38}$$

The quantity φ of (38) has the dimension of length and can be interpreted as the contribution of turbulent fluctuations of the electron number density to the overall eikonal (*i.e.*, the phase path of the waves, see [3, Chapter I]). As $\langle \mu \rangle = 0$, formula (38) yields $\langle \varphi \rangle = 0$. Given the definition of φ (38), we can recast formula (37) as

$$\mathfrak{T}_{\mathrm{ph}}(\boldsymbol{x}^n, \boldsymbol{z}) = \frac{R_z^n}{\bar{v}_{\mathrm{ph}}} - \frac{\varphi_n}{2c}, \quad \mathfrak{T}_{\mathrm{gr}}(\boldsymbol{x}^n, \boldsymbol{z}) = \frac{R_z^n}{\bar{v}_{\mathrm{gr}}} + \frac{\varphi_n}{2c}, \quad \text{where} \quad \varphi_n \equiv \varphi(\boldsymbol{x}^n, \boldsymbol{z}) = \frac{4\pi e^2}{m_{\mathrm{e}} \omega_0^2} \int_0^{R_z^n} \mu(\boldsymbol{x}(r))\, dr. \tag{39}$$

Statistics of propagation through a turbulent medium. The variance of the eikonal (or, more precisely, the variances of the quantities φ^n given by (39)) will play a key role in estimating the effect of ionospheric turbulence on spaceborne SAR imaging. Those variances are determined by the statistics of the turbulent medium. A convenient way to characterize the latter is to introduce the correlation function of the random field $\mu(\boldsymbol{x})$ of (36):

$$V(\boldsymbol{x}', \boldsymbol{x}'') \stackrel{\mathrm{def}}{=} \langle \mu(\boldsymbol{x}') \mu(\boldsymbol{x}'') \rangle\,. \tag{40}$$

Note that $\boldsymbol{x}'$ and $\boldsymbol{x}''$ in formula (40) may be arbitrary points in $\mathbb{R}^3$, not necessarily on the orbit. Since the random field $\mu(\boldsymbol{x})$ is homogeneous and isotropic, the correlation function (40) becomes a function of one scalar variable, the distance r between $\boldsymbol{x}'$ and $\boldsymbol{x}''$:

$$V(\boldsymbol{x}', \boldsymbol{x}'') = \langle \mu^2 \rangle V_r(r), \qquad r = |\boldsymbol{x}' - \boldsymbol{x}''|,$$

where $\langle \mu^2 \rangle = \mathrm{const}$. This setting parallels the simplified deterministic setting of Section 3 in that it does not take into account the inhomogeneity of the medium along the ray path, a feature that the actual Earth's ionosphere does have.

Henceforth, we will consider only short-range correlation functions of the medium $V_r(r)$, *i.e.*, those that decay rapidly as r increases. The simplest one is the exponentially decaying correlation function:

$$V_r(r) = e^{-r/r_0}, \tag{41}$$

where r_0 is the medium correlation radius. Two more examples that have been investigated in [1, Appendix 4.A] are the Gaussian correlation function and the Kolmogorov-Obukhov correlation function.

The variance of the eikonal or, equivalently, the variance of the quantity φ defined by (38), is given by the following expression:

$$\begin{aligned} \left\langle \varphi^2 \right\rangle &= \left(\frac{4\pi e^2}{m_{\mathrm{e}} \omega_0^2} \right)^2 \left\langle \int_0^{R_z} \mu(\boldsymbol{x}(r'))dr' \cdot \int_0^{R_z} \mu(\boldsymbol{x}(r''))dr'' \right\rangle \\ &= \left(\frac{4\pi e^2}{m_{\mathrm{e}} \omega_0^2} \right)^2 \int_0^{R_z} \int_0^{R_z} \langle \mu(\boldsymbol{x}(r')) \mu(\boldsymbol{x}(r'')) \rangle\, dr'\, dr'' = \left(\frac{4\pi e^2}{m_{\mathrm{e}} \omega_0^2} \right)^2 \langle \mu^2 \rangle \int_0^{R_z} \int_0^{R_z} V_r(|r' - r''|)\, dr'\, dr'', \end{aligned} \tag{42}$$

where the integration in every instance is performed along the straight line between $\boldsymbol{x}$ and $\boldsymbol{z}$. Due to the rapid decay of V_r, the second integral on the last line of (42) is dominated by the pairs (r', r'') such that $|r' - r''| \lesssim r_0 \ll R_z$. For the exponentially decaying correlation function (41), we have:

$$\left\langle \varphi^2 \right\rangle \approx 2R_z r_0 \frac{\langle \mu^2 \rangle}{\langle N_e \rangle^2} \left(\frac{\bar{\omega}_{pe}^2}{\omega_0^2} \right)^2 . \tag{43}$$

According to (43), the variation of $\langle \varphi_n^2 \rangle$ in n is due to the variation of the travel distance R_z^n. The latter is described by

$$\frac{|R_z^n - R|}{R} \lesssim \frac{1}{8} \frac{L_{SA}^2}{R^2} \ll 1.$$

Therefore, in our subsequent analysis we will not be distinguishing between the variances $\langle \varphi_n^2 \rangle$ for different values of n within the synthetic array. It will be convenient to introduce a new parameter $\mathcal{D}^2$ that will actually describe the effect of ionospheric turbulence on the GAF of the SAR system:

$$\mathcal{D}^2 \stackrel{\text{def}}{=} \frac{1}{2} \frac{\omega_0^2}{c^2} \left\langle \varphi_n^2 \right\rangle \approx \frac{\omega_0^2}{c^2} R r_0 \frac{\langle \mu^2 \rangle}{\langle N_e \rangle^2} \left(\frac{\bar{\omega}_{pe}^2}{\omega_0^2} \right)^2 . \tag{44}$$

From (44), it is easy to see that $\mathcal{D}^2 \propto \frac{\langle \varphi_n^2 \rangle}{\lambda_0^2}$, so the meaning of $\mathcal{D}$, up to a constant factor, is the ratio of the standard deviation of the eikonal (which is the same for all n) to the carrier wavelength. Equivalently, $\mathcal{D}$ can be thought of as the standard deviation of the signal travel time relative to the period of the carrier oscillations.

To assess the performance of a SAR system in the case of imaging through a turbulent ionosphere, it will be necessary to introduce the stochastic GAF and compute its certain statistical averages (*i.e.*, moments). This is done in Sections 4.2 through 4.5. However, having only the expressions for the variances $\left\langle \varphi_n^2 \right\rangle$ proves insufficient for that purpose. In addition, we assume that for sufficiently large integration distances R_z^n, each quantity φ_n becomes a zero-mean Gaussian random variable. This is an implication of the central (or classical) limit theorem [6, Chapter 8], because the integration path in (39) crosses through many identically distributed inhomogeneities, see [3, Chapter I]. In Sections 4.3, 4.4, and 4.5, we will need the following expression:

$$\left\langle e^{-i\frac{\omega_0}{c}\varphi_n} \right\rangle = \frac{1}{\sqrt{2\pi \langle \varphi_n^2 \rangle}} \int e^{-i\frac{\omega_0}{c}\mathfrak{u}} e^{-\frac{\mathfrak{u}^2}{2\langle \varphi_n^2 \rangle}} d\mathfrak{u} = e^{-\frac{\omega_0^2}{2c^2}\langle \varphi_n^2 \rangle} = e^{-\mathcal{D}^2}. \tag{45}$$

In addition to the statistics of individual eikonals φ_n, we will need a way to characterize the correlation between them. We assume that the eikonals also exhibit a short-range correlation with the radius r_φ. It is shown in [3, Chapter I] that if the fluctuations of the phase are small, then for planar propagation we have $r_\varphi \sim r_0$. Although the geometry of signal propagation for SAR imaging is more complex, this result remains generally true (see [1, Appendix 4A] for more detail). In the case of large fluctuations of the phase (see Section 4.3.3), we refer to [7] for justification.

In order to actually quantify the correlation between the propagation phases, we introduce a normalized correlation function of the eikonal:

$$f_{mn} \equiv f(\mathfrak{y}_{mn}) \stackrel{\text{def}}{=} \frac{\langle \zeta_m \zeta_n \rangle}{\langle \zeta_n^2 \rangle} = \frac{\langle \varphi_m \varphi_n \rangle}{\langle \varphi_n^2 \rangle}, \quad \text{where} \quad \mathfrak{y}_{mn} = \frac{|\boldsymbol{x}^m - \boldsymbol{x}^n|}{r_\varphi} . \tag{46}$$

The quantities f_{mn} can also be thought of as the entries of a matrix referred to as the covariance matrix of the random variables φ_n. In addition, we will need to assume that the random variables φ_n are jointly Gaussian, *i.e.*, described by a multivariate Gaussian probability density function (note that this is a separate assumption; it goes beyond the previous one that all individual phases are Gaussian random variables). Based on this assumption, it can be shown that

$$\langle e^{-i\frac{\omega_0}{c}(\varphi_m - \varphi_n)} \rangle = e^{-2\mathcal{D}^2(1 - f_{mn})}. \tag{47}$$

Expression (47) will prove useful in Sections 4.3, 4.4, and 4.5.

4.2 Stochastic GAF

4.2.1 General formulation and range-azimuth factorization

Suppose we are using the filter that is corrected for the deterministic part of the electron number density in the sense of Section 3.3, *i.e.*, the plasma frequency in the filter is based on $\langle N_e \rangle$, see (36). Accordingly, we introduce the notation similar to $T^n_{\mathrm{gr,ph}}$ in (21) but with the random contributions to the travel times taken into account as in (39):

$$\begin{aligned} T'^n_{\mathrm{ph}} &= \frac{R^n_y}{\bar{v}_{\mathrm{ph}}} - \mathfrak{T}_{\mathrm{ph}}(\boldsymbol{x}^n, \boldsymbol{z}) = \frac{R^n_y - R^n_z}{\bar{v}_{\mathrm{ph}}} + \frac{\varphi_n}{2c}, \\ T'^n_{\mathrm{gr}} &= \frac{R^n_y}{\bar{v}_{\mathrm{gr}}} - \mathfrak{T}_{\mathrm{gr}}(\boldsymbol{x}^n, \boldsymbol{z}) = \frac{R^n_y - R^n_z}{\bar{v}_{\mathrm{ph}}} - \frac{\varphi_n}{2c}. \end{aligned} \tag{48}$$

We have

$$2\omega_0 T'^n_{\mathrm{ph}} = 2\omega_0\Big(\frac{R^n_y - R^n_z}{\bar{v}_{\mathrm{ph}}} + \frac{\varphi_n}{2c}\Big) = 2\frac{\omega_0}{B}B\frac{\bar{v}_{\mathrm{gr}}}{\bar{v}_{\mathrm{ph}}}\Big(\frac{R^n_y - R^n_z}{\bar{v}_{\mathrm{gr}}} + \frac{\bar{v}_{\mathrm{ph}}}{\bar{v}_{\mathrm{gr}}}\frac{\varphi_n}{2c}\Big) \tag{49}$$

and

$$2\alpha\tau T'^n_{\mathrm{gr}} = B\Big(\frac{R^n_y - R^n_z}{\bar{v}_{\mathrm{gr}}} - \frac{\varphi_n}{2c}\Big). \tag{50}$$

In (49) and (50), we have kept only the leading terms in both the deterministic and stochastic components. Unlike (8), the quantities $T'^n_{\mathrm{ph,gr}}$ of (48) do not vanish when $\boldsymbol{y} = \boldsymbol{z}$, which indicates the presence of a mismatch between the filter (35) and the signal that propagates through a turbulent ionosphere where the travel times are given by (37). This mismatch is due to the stochastic term $\mu(\boldsymbol{x})$ in (36). The right-hand side of formula (49) can be compactly represented as

$$2\frac{\omega_0}{B}\frac{\bar{v}_{\mathrm{gr}}}{\bar{v}_{\mathrm{ph}}}\Big(B\frac{R^n_y - R^n_z}{\bar{v}_{\mathrm{gr}}} + \frac{\bar{v}_{\mathrm{ph}}}{\bar{v}_{\mathrm{gr}}}\frac{B\varphi_n}{2c}\Big) = w(\xi + \eta n + \zeta_n).$$

On the right-hand side of the previous formula, ξ and η are two dimensionless parameters that characterize the shift between $\boldsymbol{y}$ and $\boldsymbol{z}$ in range and azimuth, respectively, $\{\zeta_n\}$ are dimensionless random variables [cf. formula (8)]:

$$\xi = \frac{B(y_2 - z_2)}{\bar{v}_{\mathrm{gr}}}\frac{L}{R}, \quad \eta = -\frac{B(y_1 - z_1)L_{\mathrm{SA}}}{\bar{v}_{\mathrm{gr}}RN}, \quad \zeta_n = \frac{\bar{v}_{\mathrm{ph}}}{\bar{v}_{\mathrm{gr}}}\frac{B\varphi_n}{2c}, \tag{51}$$

and w is a large dimensionless parameter:

$$w = 2\frac{\omega_0}{B}\frac{\bar{v}_{\mathrm{gr}}}{\bar{v}_{\mathrm{ph}}}, \quad \text{such that} \quad \mathcal{D}^2 = \frac{w^2\langle\zeta_n^2\rangle}{2}, \tag{52}$$

see (44). Using the same notations, we can also rewrite (50) as

$$B\Big(\frac{R^n_y - R^n_z}{\bar{v}_{\mathrm{gr}}} - \frac{\varphi_n}{2c}\Big) = \xi + \eta n - \frac{\bar{v}_{\mathrm{gr}}}{\bar{v}_{\mathrm{ph}}}\zeta_n.$$

Then, the expression for the GAF takes the following form:

$$W'(\xi,\eta) = \sum_n W'_n(\xi,\eta) \approx \sum_n e^{-2i\omega_0 T'^n_{\mathrm{ph}}}\int_{-\tau/2}^{\tau/2} e^{-4i\alpha T'^n_{\mathrm{gr}}t}dt = \sum_n e^{-iw(\xi+\eta n+\zeta_n)}\tau\,\mathrm{sinc}\,(\xi + \eta n - \frac{\bar{v}_{\mathrm{gr}}}{\bar{v}_{\mathrm{ph}}}\zeta_n), \tag{53}$$

Additional corroboration of this formula can be found in [7], where a multiscale approach to the propagation through random media has been adopted.

In (53), we have neglected the modification of the chirp rate due to the turbulence; it can be shown that this effect is weaker than the one due to the modification of the travel times. We see that unless a given realization of the random sequence $\{\zeta_n\}$ happens to be linear with respect to n (special case), the overall complex phase under the sum on the right-hand side of (53) is not linear with respect to n either. This may be interpreted as a mismatch in azimuth.

When $\zeta_n \equiv 0$ in (53), the expression for the stochastic GAF reduces to that for a previously studied deterministic GAF:

$$W(\xi,\eta) = \sum_n W_n(\xi,\eta) \approx \sum_n e^{-iw(\xi+\eta n)}\tau\,\mathrm{sinc}(\xi+\eta n). \tag{54}$$

The GAF (54) admits an approximate factorized representation:

$$W_{(\mathrm{R}\Sigma)}(\xi,\eta) = \tau N e^{-iw\xi}\,\mathrm{sinc}(\xi)\,\mathrm{sinc}\Big(\frac{w\eta N}{2}\Big). \tag{55}$$

Formula (55) coincides with (11) up to the choice of notation. We will apply a similar factorization procedure to the stochastic GAF $W'(\xi,\eta)$ defined by (53). Due to the presence of random variables ζ_n, $W'(\xi,\eta)$ is a random function of its arguments. The variables ζ_n enter formula (53) in two different ways. In the exponent of each term W'_n, they yield a random phase shift by $w\zeta_n$, which combines with the deterministic term $w\eta n$ that is proportional to n. The second occurrence of ζ_n is via the argument of the sinc function in (53). However, in the factorized representation of the stochastic GAF $W'(\xi,\eta)$, the random variables ζ_n under the $\mathrm{sinc}(\,\cdot\,)$ on the right-hand side of (53) will be disregarded. This yields, similarly to the deterministic factorization (55):

$$W'_{(\mathrm{R}\Sigma)}(\xi,\eta) \stackrel{\mathrm{def}}{=} \tau e^{-iw\xi}\,\mathrm{sinc}(\xi)\sum_n e^{-iw(\eta n+\zeta_n)}. \tag{56}$$

4.2.2 Assessing image quality in the stochastic framework

The randomness of the function $W'(\xi,\eta)$ defined by formula (53) means that for every pair of arguments (ξ,η) the quantity $W'(\xi,\eta)$ is a random variable. Generally speaking, if the multivariate probability density of the set of random variables $\{\zeta_n\}$ in known, then one can calculate the probability density for $W'(\xi,\eta)$. However, with the number of variables ζ_n in the hundreds or thousands, this approach does not seem practical for the nonlinear expression (53). Instead, to evaluate the effect of turbulence we will use a distance between the perturbed and unperturbed GAF:

$$\mathrm{dist}(W', W). \tag{57}$$

One possibility to define the distance (57) is to introduce the difference:

$$\delta W(\xi,\eta) = W'(\xi,\eta) - W(\xi,\eta), \tag{58}$$

where $W(\xi,\eta)$ is the deterministic GAF given by (54), and consider the first and second moments of δW. The contribution of the first moment (*i.e.*, mean) of δW into the smearing of the main lobe of the GAF can be evaluated as follows [cf. Section 2.3]:

$$\frac{|\text{mean value at the edge of the main lobe}|}{|\text{value at the central maximum}|} = \frac{\max\big|_{W=0}|\langle\delta W\rangle|}{\max|W|}.$$

As the values of W of (54) are small at the zeros of $W_{(\mathrm{R}\Sigma)}$ given by (55), and the maximum values of $|W|$ and $W_{(\mathrm{R}\Sigma)}$ coincide, we can calculate $\langle\delta W\rangle$ at the zeros of $W_{(\mathrm{R}\Sigma)}$ instead:

$$\frac{|\text{mean value at the edge of the main lobe}|}{|\text{value at the central maximum}|} \approx \frac{\max\big|_{W_{(\mathrm{R}\Sigma)}=0}|\langle\delta W\rangle|}{\max|W_{(\mathrm{R}\Sigma)}|}. \tag{59}$$

Next, we define the variance of δW: $\sigma^2_{\delta W} = \langle|\delta W - \langle\delta W\rangle|^2\rangle$. The standard deviation $\sqrt{\sigma^2_{\delta W}}$ at such (ξ,η) that $W(\xi,\eta) = 0$ may be interpreted as the statistically averaged smearing of the ambiguity function $W(\xi,\eta)$, similarly to how the factorization error smears the zeros of $W_{(\mathrm{R}\Sigma)}(\xi,\eta)$. Similarly to (59), we calculate the variance at the zeros of $W_{(\mathrm{R}\Sigma)}$:

$$\frac{|\text{RMS variation at the edge of the main lobe}|}{|\text{value at the central maximum}|} \approx \frac{\sqrt{\sigma^2_{\delta W}}\Big|_{W_{(\mathrm{R}\Sigma)}=0}}{\max|W_{(\mathrm{R}\Sigma)}|}. \tag{60}$$

One type of zeros of $W_{(\mathrm{R}\Sigma)}$ to be considered in (59) and (60) corresponds to the edges of the main lobe in range: $\xi = \pm\pi$. At these locations, $W'_{(\mathrm{R}\Sigma)}$ is also zero; hence, the variance of W' is the same as that of $W' - W'_{(\mathrm{R}\Sigma)}$. This

variance may be called the factorization error of W'. The other type of zeros of $W_{(\mathrm{R}\Sigma)}$ correspond to the edges of the main lobe in azimuth: $\eta = \pm 2\pi/(Nw)$. There, $W'_{(\mathrm{R}\Sigma)}$ is not necessarily zero. This suggests rewriting formula (58) as

$$\delta W = (W' - W'_{(\mathrm{R}\Sigma)}) + (W'_{(\mathrm{R}\Sigma)} - W_{(\mathrm{R}\Sigma)}) + (W_{(\mathrm{R}\Sigma)} - W) = \underbrace{(W'_{(\mathrm{R}\Sigma)} - W_{(\mathrm{R}\Sigma)})}_{\delta W_1} + [\underbrace{(W' - W'_{(\mathrm{R}\Sigma)})}_{\delta W_{2a}} - \underbrace{(W - W_{(\mathrm{R}\Sigma)})}_{\delta W_{2b}}]. \tag{61}$$

The dependence of δW_1 on the range variable ξ is deterministic, see (56) and (55). Hence, this term will contribute only to the effect of turbulence on the imaging in azimuth, see Section 4.3. The factorization-related term $\delta W_2 = \delta W_{2a} - \delta W_{2b}$ turns out much smaller than δW_1, see Section 4.5. Accordingly, the conclusion will be that the effect of turbulence on the imaging in range described by δW_2 is much smaller than that on the imaging in azimuth described predominantly by δW_1.

We will see however that in the case of large-scale turbulence, the approach based on δW of (58) does not adequately describe the effect of ionospheric turbulence on image properties at all. We develop and discuss an alternative approach in Section 4.4. This is the main new result of the current paper.

4.3 The Effect of Small-scale Turbulence on Imaging in Azimuth

We will consider the effect of randomness on the imaging in azimuth as described by the term $\delta W_1 = W'_{(\mathrm{R}\Sigma)} - W_{(\mathrm{R}\Sigma)}$ in formula (61), leaving the analysis of other effects until Sections 4.4 and 4.5.

4.3.1 Mean and variance of δW_1

Let us define:

$$W'_{\mathrm{A}}(\eta) \stackrel{\text{def}}{=} \frac{1}{\tau} W'_{(\mathrm{R}\Sigma)}(0, \eta) = \sum_n W'_{\mathrm{A},n}(\eta) \approx \int_{-N/2}^{N/2} W'_{\mathrm{A},n}(\eta)\, dn, \tag{62}$$

where

$$W'_{\mathrm{A},n}(\eta) \stackrel{\text{def}}{=} e^{-iw(\eta n + \zeta_n)}. \tag{63}$$

Similarly, we define in accordance with (54)–(55):

$$W_{\mathrm{A}}(\eta) \stackrel{\text{def}}{=} \frac{1}{\tau} W_{(\mathrm{R}\Sigma)}(0, \eta) = \sum_n W_{\mathrm{A},n}(\eta) \approx \int_{-N/2}^{N/2} W_{\mathrm{A},n}(\eta)\, dn, \quad \text{where} \quad W_{\mathrm{A},n}(\eta) \stackrel{\text{def}}{=} e^{-iw\eta n},$$

so that

$$W_{\mathrm{A}}(\eta) = N \operatorname{sinc}(w\eta N/2). \tag{64}$$

Hence,

$$\delta W_1(\xi, \eta) = W'_{(\mathrm{R}\Sigma)}(\xi, \eta) - W_{(\mathrm{R}\Sigma)}(\xi, \eta) = \tau e^{-iw\xi} \operatorname{sinc} \xi \cdot (W'_{\mathrm{A}}(\eta) - W_{\mathrm{A}}(\eta)). \tag{65}$$

From equation (45), we get

$$\left\langle W'_{\mathrm{A},n}(\eta) \right\rangle = e^{-iw\eta n} e^{-\mathcal{D}^2}, \tag{66}$$

where $\mathcal{D}^2$ is introduced in (44). Consequently,

$$\langle W'_{\mathrm{A}}(\eta) \rangle = e^{-\mathcal{D}^2} W_{\mathrm{A}}(\eta). \tag{67}$$

In formula (66), we can observe a decrease in the amplitude of the mean value of each term in the sum (62) (and, hence, that of the entire sum (67)) due to random phase perturbations. This phenomenon is sometimes referred to as extinction, see [3, Chapter I].

From (66) and (67), we have:

$$\langle \delta W_1(\eta) \rangle = \tau e^{-iw\xi} \operatorname{sinc} \xi \cdot (\langle W'_{\mathrm{A}}(\eta) \rangle - W_{\mathrm{A}}(\eta)) = \tau e^{-iw\xi} \operatorname{sinc} \xi \cdot (e^{-\mathcal{D}^2} - 1) W_{\mathrm{A}}(\eta). \tag{68}$$

Expression (68) vanishes at the edge of the main azimuthal lobe of the deterministic GAF because it is proportional to $W_{\mathrm{A}}(\eta) \approx \operatorname{sinc} \frac{w\eta N}{2}$; hence, its contribution to the smearing according to (59) is zero. Obviously, the shape of $\langle W'_{\mathrm{A}}(\eta) \rangle$

in (67) is the same as that of $W_{\mathrm{A}}(\eta)$, so there is no change in azimuthal resolution either. It will be shown later that the interpretation of (67) in the context of image intensity will be different for small-scale ($r_\varphi \ll L_{\mathrm{SA}}$) and large-scale ($L_{\mathrm{SA}} \ll r_\varphi$) turbulence.

Next, we will calculate the variance of δW_1 taking into account that W_{A} is deterministic:

$$\sigma^2_{\delta W_1} = \tau^2 \operatorname{sinc}^2 \xi \cdot \left\langle |W'_{\mathrm{A}} - \langle W'_{\mathrm{A}} \rangle|^2 \right\rangle = \tau^2 \operatorname{sinc}^2 \xi \cdot \sigma^2_{W'_{\mathrm{A}}}. \tag{69}$$

In turn, the variance of W'_{A}, which is denoted by $\sigma^2_{W'_{\mathrm{A}}}$ in equation (69), can be obtained with the help of (66) in the following form (see, *e.g.*, [8, Theorem 5.10.11]):

$$\sigma^2_{W'_{\mathrm{A}}} = \left\langle \left| \sum_n (W'_{\mathrm{A},n} - e^{-\mathcal{D}^2} W_{\mathrm{A},n}) \right|^2 \right\rangle = \sum_n C_{mn}, \tag{70}$$

where

$$C_{mn} = \left\langle (e^{-iw(\eta m+\zeta_m)} - e^{-\mathcal{D}^2} e^{-iw\eta m})(e^{iw(\eta n+\zeta_n)} - e^{-\mathcal{D}^2} e^{iw\eta m}) \right\rangle = e^{-iw\eta(m-n)} \left(\langle e^{-iw(\zeta_m-\zeta_n)} \rangle - e^{-2\mathcal{D}^2} \right)$$

is the covariance matrix of the random variables (63). Using (47), we can write:

$$C_{mn} = e^{-iw\eta(m-n)} e^{-2\mathcal{D}^2} [e^{2\mathcal{D}^2 f_{mn}} - 1]. \tag{71}$$

Therefore,

$$\sigma^2_{W'_{\mathrm{A}}} = e^{-2\mathcal{D}^2} \sum_{m,n} e^{-iw\eta(m-n)} [e^{2\mathcal{D}^2 f_{mn}} - 1]. \tag{72}$$

4.3.2 Small-scale turbulence with small phase perturbations: $r_\varphi \ll L_{SA}$, $\mathcal{D} \ll 1$

This setting has been analyzed in [1, Chapter 4]. First, consider the case where the random variables ζ_n (or, equivalently, φ_n) are uncorrelated, *i.e.*, $f_{mn} = \delta_{mn}$, see (46). From the standpoint of practice, this case is not realistic: it requires that the correlation radius of the medium r_φ be much shorter not only than the synthetic aperture L_{SA}, but also than the distance between the successive emitting/receiving locations of the antenna on the orbit:

$$r_\varphi \ll |\boldsymbol{x}^{n+1} - \boldsymbol{x}^n| = \frac{L_{\mathrm{SA}}}{N} \tag{73}$$

The distance $|\boldsymbol{x}^{n+1} - \boldsymbol{x}^n|$ is on the order of antenna size, see [1, Section 2.4.2], which is much shorter than the typical values of the correlation radius of ionospheric turbulence, as reported, *e.g.*, in [9, 10]. We present the analysis of this case for the sake of completeness.

For a diagonal covariance matrix C_{mn}, formulae (70) and (72) yield:

$$\sigma^2_{W'_{\mathrm{A}}} = e^{-2\mathcal{D}^2} \sum_n [e^{2\mathcal{D}^2 f_{mn}} - 1] = N e^{-2\mathcal{D}^2} [e^{2\mathcal{D}^2} - 1] \approx N \cdot 2\mathcal{D}^2. \tag{74}$$

Hence, the variance of W'_{A} given by (74) appears independent of the azimuthal variable η. Its contribution to the smearing of the main lobe of the GAF estimated according to (60) with the help of (69) is

$$\frac{\sqrt{\tau^2 \sigma^2_{W'_{\mathrm{A}}}}}{N\tau} = \sqrt{\frac{2\mathcal{D}^2}{N}}. \tag{75}$$

A more realistic and more interesting case is that of intermediate values of r_φ [cf. formula (73)]:

$$|\boldsymbol{x}^{n+1} - \boldsymbol{x}^n| = \frac{L_{\mathrm{SA}}}{N} \ll r_\varphi \ll L_{\mathrm{SA}}.$$

One can expect the phases that correspond to distant locations within the synthetic array to be weakly correlated or uncorrelated, because for $|\boldsymbol{x}^m - \boldsymbol{x}^n| \gtrsim r_\varphi$ the covariance f_{mn} given by (46) is close to zero. Yet a strong correlation between signal phases should be expected for the neighboring and close to neighboring antenna positions $\boldsymbol{x}^m$ and $\boldsymbol{x}^n$ that satisfy $|\boldsymbol{x}^m - \boldsymbol{x}^n| = |m-n| \frac{L_{\mathrm{SA}}}{N} \ll r_\varphi$. Indeed, for $\mathfrak{v}_{mn} = |\boldsymbol{x}^m - \boldsymbol{x}^n| / r_\varphi \ll 1$ we have $f_{mn} \equiv f(\mathfrak{v}_{mn}) \approx f(0) = 1$.

To compute the variance $\sigma^2_{W'_{\mathrm{A}}}$ given by (72), we take into account that within the main azimuthal lobe we have $|w\eta| \sim \frac{1}{N} \ll 1$, see (55), and replace the sum on the right-hand side of (72) with a double integral:

$$\sigma^2_{W'_{\mathrm{A}}} \approx e^{-2\mathcal{D}^2} \int_{-N/2}^{N/2} dm \int_{-N/2}^{N/2} dn\, e^{-iw\eta(m-n)}[e^{2\mathcal{D}^2 f_{mn}} - 1]. \tag{76}$$

Then, we change the integration variables in (76) from (m, n) to

$$\mathfrak{u} = m - n, \quad \mathfrak{v} = m + n, \quad \frac{\partial(\mathfrak{u}, \mathfrak{v})}{\partial(m, n)} = 2.$$

As the integrand in (76) depends only on $\mathfrak{u}$ we can write:

$$\int_{-N/2}^{N/2} dm \int_{-N/2}^{N/2} dn\, f_1(\mathfrak{u}) = \frac{1}{2} \int_{-N}^{N} d\mathfrak{u}\, (2N - 2|\mathfrak{u}|) f_1(\mathfrak{u}),$$

where we have denoted

$$f_1(\mathfrak{u}) = e^{-iw\eta\mathfrak{u}}[e^{2\mathcal{D}^2 f(S\mathfrak{u})} - 1] \quad \text{and} \quad S = \frac{L_{\mathrm{SA}}}{r_\varphi N}.$$

Thus,

$$\sigma^2_{W'_{\mathrm{A}}} = e^{-2\mathcal{D}^2} \int_{-N}^{N} d\mathfrak{u}\, (N - |\mathfrak{u}|) e^{-iw\eta\mathfrak{u}}[e^{2\mathcal{D}^2 f(S\mathfrak{u})} - 1].$$

As the function f of (46) is even, we can transform the previous integral into

$$\sigma^2_{W'_{\mathrm{A}}} = 2e^{-2\mathcal{D}^2} \int_{0}^{N} d\mathfrak{u}\, (N - \mathfrak{u}) \cos(w\eta\mathfrak{u})[e^{2\mathcal{D}^2 f(S\mathfrak{u})} - 1] \approx 4\mathcal{D}^2 \int_{0}^{N} d\mathfrak{u}\, (N - \mathfrak{u}) \cos(w\eta\mathfrak{u}) f(S\mathfrak{u}). \tag{77}$$

Since $f(\mathfrak{y})$ decays rapidly for $\mathfrak{y} \gtrsim 1$, the factor $f(S\mathfrak{u})$ in the integrand of (77) is non-negligible only where its argument $S\mathfrak{u}$ is not large:

$$|\mathfrak{u}| \lesssim \frac{1}{S} = \frac{r_\varphi N}{L_{\mathrm{SA}}} \ll N. \tag{78}$$

Then, expression (77) simplifies to

$$\sigma^2_{W'_{\mathrm{A}}}(\eta) \approx 4\mathcal{D}^2 N \int_{0}^{N} d\mathfrak{u}\, \cos(w\eta\mathfrak{u}) f(S\mathfrak{u}). \tag{79}$$

As long as (78) holds, for the argument of $\cos(w\eta\mathfrak{u})$ in (79) we have:

$$|w\eta\mathfrak{u}| \lesssim \left|\frac{w\eta}{S}\right| = \left|\frac{w\eta r_\varphi N}{L_{\mathrm{SA}}}\right| \ll |w\eta N|.$$

We are interested in the values of η that correspond to the main lobe of the GAF in azimuth: $|w\eta N| \leqslant 2\pi$, see (55). Hence, the argument of cosine in (79) is small, and to the leading order we can take $\cos(w\eta\mathfrak{u}) \approx 1$. Moreover, as $SN = L_{\mathrm{SA}}/r_\varphi \gg 1$, the rapid decay of $f(S\mathfrak{u})$ for large $S\mathfrak{u}$ allows us to replace the upper limit of integration in (79) with infinity:

$$\sigma^2_{W'_{\mathrm{A}}} \approx \frac{4\mathcal{D}^2 N}{S} \int_{0}^{\infty} f(\mathfrak{u})\, d\mathfrak{u} = \frac{4\mathcal{D}^2 N}{S}. \tag{80}$$

The last equality in (80) holds because the correlation function of the eikonal as a function of r is defined as $f(r/r_\varphi)$, see (46). Consequently, the smearing effect of randomness on the GAF evaluated in accordance with (60) for the variance $\sigma^2_{W'_\mathrm{A}}$ given by (80) is

$$\frac{\sqrt{\tau^2\sigma^2_{W'_\mathrm{A}}}}{N\tau} = \sqrt{\frac{4\mathcal{D}^2}{L_\mathrm{SA}/r_\varphi}}\,. \tag{81}$$

Since $L_\mathrm{SA}/r_\varphi \ll N$, the quantity on the right-hand side of (81) is much larger than that on the right-hand side of (75). As the variance (80) does not depend on η, the smearing is constant along the azimuthal coordinate, similarly to case of independent random phases, see (74). Comparing formulae (75) and (81), we see that the main difference is that the quantity N in the denominator under the square root on the right-hand side of (75) is replaced with L_SA/r_φ in (81). One can therefore interpret L_SA/r_φ in (81) as the number of "independent clusters," whereas in (75) all N individual phases are independent. Each cluster can be thought of as composed of the phases in a segment of length r_φ that are strongly correlated with each other and hence can be represented by one Gaussian random variable. On the other hand, the correlation beyond a given cluster is weak, so the random phases from different clusters can be considered independent. Accordingly, the phase perturbations from different clusters tend to average out. The shorter the correlation radius r_φ compared to the synthetic aperture (*i.e.*, the larger the number of uncorrelated clusters L_SA/r_φ), the weaker the smearing of the azimuthal GAF.

For the peak height, we have

$$\langle|W'_\mathrm{A}(0)|^2\rangle = \Big\langle \sum_{m,n} e^{-iw(\zeta_n-\zeta_m)}\Big\rangle = \sum_{m,n} e^{-2\mathcal{D}^2(1-f_{mn})}, \tag{82}$$

see (62)–(63). As long as $r_\varphi \ll L_\mathrm{SA}$ (which is true for both uncorrelated and clustered ζ_n), most of the terms f_{mn} in the sum on the right-hand side of (82) are small and, consequently, the corresponding exponents are approximately $e^{-2\mathcal{D}^2}$. Hence, the value of the sum in (82) is consistent with (67).

4.3.3 Small-scale turbulence with large phase perturbations: $r_\varphi \ll L_{SA}$, $\mathcal{D} \gg 1$

In this section, we follow the analysis of [7]. There, it has been pointed out that when $r_\varphi \ll L_\mathrm{SA}$ and $\mathcal{D} \gg 1$, the integral in (62) is a superposition of independent components, each originating from a cluster of neighboring antenna locations of size r_φ (see (81) and the following comment). The result is a zero-mean complex Gaussian random variable with the variance of the amplitude of the order of its mean, see [11, Chapter 4] and [12]. To study the correlation properties of $W'_\mathrm{A}(\eta)$, we obtain with the help of (47):

$$\langle\overline{W'_\mathrm{A}}(\eta_a)W'_\mathrm{A}(\eta_b)\rangle = \iint_{-N/2}^{N/2}\Big\langle e^{iw(m\eta_a+\zeta_m)}e^{-iw(n\eta_b+\zeta_n)}\Big\rangle\,dm\,dn = \iint_{-N/2}^{N/2} e^{iw(m\eta_a-n\eta_b)}e^{-2\mathcal{D}^2(1-f_{mn})}dm\,dn, \tag{83}$$

where $\eta_a = -B(y_{a1}-z_1)L_\mathrm{SA}/(N\bar{v}_\mathrm{gr}R)$, $\eta_b = -B(y_{b1}-z_1)L_\mathrm{SA}/(N\bar{v}_\mathrm{gr}R)$, see (51). The second exponent on the right-hand side of (83) is not very small if f_{mn} is close to 1. Using the Taylor approximation $f(\mathfrak{v}) \approx 1 - K\mathfrak{v}^2$ for $f(\mathfrak{v})$ of (46) near zero, we can write:

$$\frac{\langle\zeta_n\zeta_m\rangle}{\langle\zeta^2\rangle} = f_{mn} \approx 1 - K\Big(\frac{x_1^m - x_1^n}{r_\varphi}\Big)^2 \approx 1 - K\frac{(m-n)^2}{N^2}\frac{L_\mathrm{SA}^2}{r_\varphi^2}\,. \tag{84}$$

As the variables ζ_n and ζ_m should decorrelate for $|\boldsymbol{x}^m - \boldsymbol{x}^n| \gtrsim r_\varphi$, we have $K \sim 1$. The effective correlation distance r_W for the terms $e^{-iw\zeta_n} = e^{-i\omega_0\varphi_n/c}$ in (83) can be found by substituting (84) into (47):

$$\mathcal{D}^2K\Big(\frac{x_1^m - x_1^n}{r_\varphi}\Big)^2 \lesssim 1, \quad \text{thus,} \quad r_W \sim \frac{r_\varphi}{\mathcal{D}}. \tag{85}$$

Performing the integration in (83) with the help of (84), we obtain:

$$\langle\overline{W'_\mathrm{A}}(\eta_a)W'_\mathrm{A}(\eta_b)\rangle \approx \sqrt{\frac{\pi}{2K}}\frac{r_\varphi}{\mathcal{D}L_\mathrm{SA}}\,\mathrm{sinc}\Big(\frac{\omega_0 L_\mathrm{SA}}{cR}(y_{a1}-y_{b1})\Big)\,e^{-\left[\frac{1}{\sqrt{2K}}\frac{r_\varphi}{DR}\frac{\omega_0}{c}\left(\frac{y_{a1}+y_{b1}}{2}-z_1\right)\right]^2}. \tag{86}$$

The exponential term on the right-hand side of (86) describes a broad peak around the scatterer position z_1. The width of the peak is much greater than Δ_A and can be interpreted as the "resolution size" if r_W of (85) were used as the

aperture length in (12). In turn, the sinc term corresponds to random fluctuations of W'_{A} on the scale of Δ_{A} inside the aforementioned peak. As compared to (64), formula (86) indicates a severe deterioration of the image of a point scatterer, which is expected.

The results given by formulae (85) and (86) will also be revisited later, see Section 5.

4.4 The Effect of Large-scale Turbulence on Imaging in Azimuth

This is the case of $L_{\mathrm{SA}} \ll r_\varphi$ where the separation between any two antenna positions within the array (not only the neighboring positions) is always smaller than the correlation length of the phase. As a result, the individual eikonals φ_n (and, hence, the variables ζ_n) are "almost correlated" with one another, and hence, the approach developed for the case of large-scale deterministic inhomogeneity, see Section 3.2.2, should be applicable. Besides, we may expect that unlike in Section 4.3.3, usable images can still be obtained even if $\mathcal{D} \gg 1$, because for $L_{\mathrm{SA}} \ll r_\varphi$ the aperture is not exposed to the full variation of the electron number density in the propagation medium. In what follows, we show that this is indeed the case; moreover, in certain situations, the only significant distortion will be an azimuthal shift of the image. Similarly to Sections 4.3.2 and 4.3.3, the key goal of this section is to characterize and quantify the image distortions resulting from the random behavior of the eikonals; however, due to the aforementioned effects, the use of the function δW of (58) for this purpose appears inadequate. To the best of our knowledge, the effect of large-scale ionospheric turbulence on spaceborne imaging has not been previously analyzed in detail in the SAR literature.

As the propagation properties change gradually on the scale of L_{SA}, for each realization of the set $\{\zeta_n\}$, see (51), we can write the following second order polynomial approximation:

$$\zeta_n \approx A_0 + A_1 n + A_2 n^2. \tag{87}$$

A qualitative characterization of this approximation will be given later, see formulae (96) and (97). In formula (87), the coefficients A_0, A_1, and A_2 are specific for each realization, which means that they are random variables. In practice, however, one most often deals with a single image. Hence, we expect that these coefficients may appear at least as useful for the analysis of image properties as the statistics of $\{\zeta_n\}$. Moreover, with the help of (38) and (51) one can observe a similarity between (87) and the deterministic formula (29). Accordingly, in this section we will describe the statistical counterparts to image distortions mentioned in Section 3.2.2, namely, the azimuthal shift and QPE-induced blurring.

To derive the coefficients A_0, A_1, and A_2 of (87) for a given realization $\{\zeta_n\}$, we employ the method of least squares. If we truncate the polynomial (87) after the first or second term, then we write:

$$A_0 = \arg\min_{\mathcal{A}_0} \sum_n (\zeta_n - \mathcal{A}_0)^2 \quad \text{or} \quad (A_0, A_1) = \arg\min_{\mathcal{A}_0, \mathcal{A}_1} \sum_n (\zeta_n - \mathcal{A}_0 - \mathcal{A}_1 n)^2,$$

respectively. The corresponding solutions are

$$A_0 = \frac{1}{N} \sum_n \zeta_n \quad \text{and} \quad A_1 = \Big(\sum_n n^2 \Big)^{-1} \sum_n n\zeta_n \tag{88}$$

(the expressions for A_0 coincide for both cases). For all three terms retained in (87), the least squares solution for A_1 is the same as in (88), while

$$\begin{aligned} A_0 &= \Big(N \sum_n n^4 - \Big(\sum_n n^2 \Big)^2 \Big)^{-1} \cdot \Big(- \sum_n n^2 \cdot \sum_n n^2 \zeta_n + \sum_n n^4 \cdot \sum_n \zeta_n \Big), \\ A_2 &= \Big(N \sum_n n^4 - \Big(\sum_n n^2 \Big)^2 \Big)^{-1} \cdot \Big(N \cdot \sum_n n^2 \zeta_n - \sum_n n^2 \cdot \sum_n \zeta_n \Big). \end{aligned} \tag{89}$$

First, we observe that the right-hand sides of all formulae (88) and (89) are linear with respect to ζ_n. Consequently,

$$\langle A_0 \rangle = \langle A_1 \rangle = \langle A_2 \rangle = 0. \tag{90}$$

The second moments of $A_{0,1,2}$ can be evaluated by considering a truncated power series for $f(\mathfrak{y})$ of (46) near zero, provided that this function is sufficiently smooth. As $f(\mathfrak{y})$ is an even function, only the even powers are present, so we

can write: $f(\mathfrak{y}) \approx 1 - K\mathfrak{y}^2 + Q\mathfrak{y}^4$, and obtain similarly to (84):

$$\frac{\langle \zeta_n \zeta_m \rangle}{\langle \zeta^2 \rangle} = f_{mn} \approx 1 - K\frac{(m-n)^2}{N^2}\frac{L_{\rm SA}^2}{r_\varphi^2} + Q\frac{(m-n)^4}{N^4}\frac{L_{\rm SA}^4}{r_\varphi^4}. \tag{91}$$

We also have $K > 0$ because $f(\mathfrak{y})$ is an autocorrelation function and therefore has a local maximum at $\mathfrak{y} = 0$. In order to show that $Q > 0$, we introduce the function of a continuous argument:

$$\zeta = \zeta(x_1) \quad \text{such that} \quad \zeta_n = \zeta(x_1^n) = \zeta\Big(n\frac{L_{\rm SA}}{N}\Big). \tag{92}$$

As mentioned at the end Section 4.1, the correlation function of ζ_n (and hence of $\zeta(x_1)$) is short-range, similarly to the correlation function of the medium described, *e.g.*, by (41). A function such as (41) clearly satisfies the necessary and sufficient condition for ergodicity known as the Slutskii theorem, see [2, Section 4.7]:

$$\lim_{S\to\infty}\frac{1}{S}\int_0^S f(\mathfrak{y})\,d\mathfrak{y} = 0.$$

Hence, we can substitute spatial averages for statistical means in the definition of f, see (46):

$$f(\mathfrak{y}) = C_f \int \zeta(x_1)\zeta(x_1 + \mathfrak{y}r_\varphi)\,dx_1, \tag{93}$$

where C_f is a normalization constant. Differentiating (93) with respect to $\mathfrak{y}$, changing the integration variable to $x_1' = x_1 + \mathfrak{y}r_\varphi$, and differentiating again, we find that $-d^2f/d\mathfrak{y}^2$ is proportional to the autocorrelation function of $d\zeta/dx_1$. Hence, $Q > 0$ because $d^2f/d\mathfrak{y}^2$ should have a local minimum at $\mathfrak{y} = 0$. Similarly to $|K| \sim 1$ in (84), we can show that $|Q| \sim 1$ from the definition of r_φ. Additionally, for $N \gg 1$, we will approximate the sums by integrals to obtain $\sum_n n^2 \approx N^3/12$ and $\sum_n n^4 \approx N^5/80$. Altogether, for the second moments of A_0 and A_1 given by (88) we have:

$$\langle A_0^2 \rangle = \langle \zeta^2 \rangle, \quad \langle A_1^2 \rangle N^2 = 2K\langle \zeta^2 \rangle \frac{L_{\rm SA}^2}{r_\varphi^2}, \tag{94}$$

while the second moments of A_0 and A_2 of (89) are

$$\langle A_0^2 \rangle = \langle \zeta^2 \rangle\Big(1 - \frac{3}{280}Q\frac{L_{\rm SA}^4}{r_\varphi^4}\Big), \quad \langle A_2^2 \rangle N^4 = 6Q\langle \zeta^2 \rangle \frac{L_{\rm SA}^4}{r_\varphi^4}\ . \tag{95}$$

The difference between the expressions for $\langle A_0^2 \rangle$ in (94) and (95) is insignificant, as expected.

As a useful illustration, one can employ the dimensional analysis to obtain rough estimates of the coefficients on the right-hand side of (87). To do so, one needs to estimate the first and second derivatives of $\zeta(x_1)$ defined in (92). The scale of $\zeta(x_1)$ and its argument are $\sqrt{\langle \zeta^2 \rangle}$ and r_φ, respectively. Therefore, with the help of (52) we get:

$$|A_0| \sim |\zeta| \sim \frac{\mathcal{D}}{w}, \quad |A_1|\frac{N}{L_{\rm SA}} \sim |\zeta'| \sim \frac{\mathcal{D}}{wr_\varphi}, \quad |A_2|\frac{N^2}{L_{\rm SA}^2} \sim |\zeta''| \sim \frac{\mathcal{D}}{wr_\varphi^2}. \tag{96}$$

The estimates in (96) are in agreement with (94)–(95).

Before using the approximation (87) for the analysis of image distortions, we need to estimate how accurate it is. The assessment can be obtained in the statistical sense, separately for the cases where one or two terms on the right-hand side of (87) are retained. Similarly to (94)–(95), we calculate:

$$\frac{1}{N\langle \zeta^2 \rangle}\Big\langle \sum_n (\zeta_n - A_0)^2 \Big\rangle \approx \frac{1}{6}K\frac{L_{\rm SA}^2}{r_\varphi^2}, \quad \frac{1}{N\langle \zeta^2 \rangle}\Big\langle \sum_n (\zeta_n - A_0 - A_1 n)^2 \Big\rangle \approx \frac{1}{30}Q\frac{L_{\rm SA}^4}{r_\varphi^4}\ . \tag{97}$$

Formulae (97) imply that for $L_{\rm SA} \ll r_\varphi$, the deviations of ζ_n from the zeroth order approximation $\zeta_n \approx A_0$ are on average much smaller than from $\zeta_n \approx 0$ (the latter may be called "no approximation at all"). Likewise, the first order

approximation $\zeta_n \approx A_0 + A_1 n$ is, in turn, much better than $\zeta_n \approx A_0$. Hence, one can say that as the number of terms in (87) increases, the accuracy improves. Besides using (87) together with the statistics of $A_{0,1,2}$ to quantify image distortions, we will also perform direct calculations using the statistics of $\{\zeta_n\}$, which will render a comparison.

Formula (87) leads to the interpretation of A_1 as an azimuthal shift of the peak of $W'_{\rm A}(\eta)$ with respect to its true position $\eta = 0$. Indeed, substituting (87) into (62)–(63), dropping the quadratic term, and performing the integration, we obtain [cf. formula (64)]:

$$W'_{\rm A}(\eta) \approx N \operatorname{sinc} \frac{w(\eta + A_1)N}{2}. \tag{98}$$

Using the definition of η from (51) and the estimate of A_1 from (94) we arrive at

$$\langle |y_1 - z_1|^2 \rangle = \Big(\frac{\bar{v}_{\rm gr} RN}{BL_{\rm SA}}\Big)^2 \langle |A_1|^2 \rangle, \quad \text{hence,} \quad \frac{\sqrt{\langle |y_1 - z_1|^2 \rangle}}{\Delta_{\rm A}} = \frac{\sqrt{K}}{\pi} \frac{\bar{v}_{\rm ph}}{c} \mathcal{D} \frac{L_{\rm SA}}{r_\varphi}. \tag{99}$$

Similarly to (31) in the deterministic case, the expected value of the magnitude of the shift in (99) can be considered as one of the quantitative characteristics of image distortions. The shift in (99) appears small (*i.e.*, smaller than the azimuthal resolution size) if $\mathcal{D}L_{\rm SA}/r_\varphi \ll 1$.

To quantify the image blurring, we first recall that in Sections 4.2.2 and 4.3.2 we have used the value of the perturbed GAF at the edge of the main lobe as a measure of image distortions. In addition, we have explained right after equation (26) that when the distortions are due to the QPE, the decrease of the peak height also allows one to quantify the smearing of the edge of the main lobe. Here, it will be more convenient to use the peak height, for which we can derive from the expression for $\mathcal{W}(0, \phi)$ in (26) that

$$\frac{\max |W|}{\max |W|_{\phi=0}} \approx 1 - \frac{2}{45}\phi^2 \quad \text{as} \quad \phi \to 0. \tag{100}$$

In this regard, we notice that the last term on the right-hand side of (87) yields the QPE

$$\phi_\zeta = w|A_2|N^2/4 \tag{101}$$

in the sum (62). This QPE has $\phi_{\rm inhom}$ of (32) as its deterministic counterpart. Hence, the distortions of the peak shape do not become substantial as long as

$$\phi_\zeta \ll 1 \Longrightarrow \mathcal{D}L_{\rm SA}^2/r_\varphi^2 \ll 1. \tag{102}$$

As $L_{\rm SA}/r_\varphi \ll 1$, we see that (102) imposes a much weaker constraint on the magnitude of $\mathcal{D}$ compared to the condition that the image be shifted (on average) by less than the resolution size $\Delta_{\rm A}$, see (99). Hence, it is possible to have a sufficiently sharp image (in the sense that $\phi_\zeta \ll 1$) even if the ionospheric fluctuations are strong ($\mathcal{D} \gg 1$) and the shift of the image is large (*i.e.*, $|y_1 - z_1| \gg \Delta_{\rm A}$). In this situation, the point-wise difference between the stochastic and deterministic GAF, see (58), may not be an appropriate measure of image distortions.

There are at least three different ways to quantify the effect of large-scale ionospheric turbulence on the peak height. To achieve a uniform treatment of these cases, we will analyze the expressions for the peak height of the GAF $W'_{\rm A}$ as $\mathcal{D} \to 0$. We are choosing this asymptotics only to facilitate the comparison. Otherwise, we can still consider certain expressions as $\mathcal{D} \gg 1$ (see, *e.g.*, the previous paragraph).

Taking the deterministic azimuthal factor $W_{\rm A}$ with the peak height equal to N as a reference, see (11), we will consider the correction terms, *i.e.*, $(1 - \langle W'_{\rm A} \rangle/N)$ and $(1 - \langle |W'_{\rm A}|^2 \rangle/N^2)$, that describe the effect of turbulence using three different formulations:

A. $\langle W'_{\rm A}(0) \rangle$ — from formula (67) we obtain the correction term $(1 - \langle W'_{\rm A}(0) \rangle/N) \sim \mathcal{D}^2$.

B. $\langle |W'_{\rm A}(0)|^2 \rangle$ — using the first two terms in the expansion (91), we obtain for $L_{\rm SA} \ll r_\varphi$ and $\mathcal{D}L_{\rm SA}/r_\varphi \ll 1$:

$$\langle |W'_{\rm A}(0)|^2 \rangle = \Big\langle \sum_{m,n} e^{-iw(\zeta_n - \zeta_m)} \Big\rangle = \sum_{m,n} e^{-2\mathcal{D}^2(1 - f_{mn})} \approx \sum_{m,n} e^{-2K\mathcal{D}^2 \frac{L_{\rm SA}^2}{r_\varphi^2} \frac{(m-n)^2}{N^2}} \approx N^2\Big(1 - \frac{1}{3}K\mathcal{D}^2 \frac{L_{\rm SA}^2}{r_\varphi^2}\Big). \tag{103}$$

Formula (103) yields the correction term:

$$1 - \frac{\langle |W'_{\rm A}(0)|^2 \rangle}{N^2} \sim \mathcal{D}^2 \frac{L_{\rm SA}^2}{r_\varphi^2}, \tag{104}$$

which is in agreement with the result obtained in [7]. Unlike in Section 4.3.2, where formula (82) was applied to small-scale turbulence, the asymptotics given by (103) differs significantly from that in the case A (note the small factor $L_{\rm SA}^2/r_\varphi^2$).

C. $\langle|W'_{\rm A}(-A_1)|^2\rangle$ — the QPE-based formula (100) combined with the second equation of (95) yields:

$$1-\frac{\langle|W'_{\rm A}(-A_1)|^2\rangle}{N^2}\approx\frac{4}{45}\langle\phi_\zeta^2\rangle=\frac{1}{15}Q\mathcal{D}^2\frac{L_{\rm SA}^4}{r_\varphi^4}. \tag{105}$$

The same result can be obtained by directly evaluating the asymptotics of

$$\langle|W'_{\rm A}(-A_1)|^2\rangle=\left\langle\Big|\sum_n e^{-iw(\zeta_n-A_1)}\Big|^2\right\rangle \tag{106}$$

as $\mathcal{D}\to 0$, with A_1 given by (88), and under an additional assumption that the set $\{\zeta_n\}$ is described by the multivariate Gaussian probability law (see the discussion at the end of Section 4.1). The correction term given by formula (105) is $\sim\mathcal{D}^2L_{\rm SA}^4/r_\varphi^4$, which is smaller than that in the case B by another factor of $r_\varphi^2/L_{\rm SA}^2$.

The foregoing discrepancies can be reconciled by giving a physical interpretation to the different terms in formula (87). The correction term in the case A that is based on formula (67) is due to A_0. This can be seen if we consider the limit $r_\varphi\to\infty$ that results in $f_{mn}\equiv 1$, see (84) or (91). Combined with $\langle\zeta_n^2\rangle=\langle\zeta^2\rangle=$ const, it means that all turbulent contributions to the eikonals are identical random variables: $\varphi_n=\varphi_0$, so all images in the statistical ensemble differ by a common phase factor

$$e^{-iwA_0}\equiv e^{-i\omega_0\varphi_0/c}, \tag{107}$$

such that $W'_{\rm A}(0)=Ne^{-iwA_0}$, see (62)–(63). Hence, in the case A we are dealing with the average of this phase factor over the ensemble of images.

Unlike (67), formula (103) derived in the case B does not incorporate the effect of A_0 because the common phase term e^{-iwA_0} factors out of the sum (62) and then disappears when $|W'_{\rm A}|^2$ is calculated. Other than the common phase, the turbulence results in the azimuthal shift and QPE-related decrease of the peak height of $W'_{\rm A}(\eta)$. The combined effect can be understood with the help of formula (26) if the expansion is generalized to the case of small κ:

$$|\mathcal{W}(\kappa,\phi)|\approx 1-\frac{1}{6}\kappa^2-\frac{2}{45}\phi^2. \tag{108}$$

In order to use formula (108) for the evaluation of $W'_{\rm A}$ from (62)–(63) when $\eta=0$ and ζ_n is given by (87), we should substitute $\kappa=wA_1N/2$ and $\phi=\phi_\zeta$, see (98) and (101). From (94)–(95), we observe that $\phi_\zeta^2\sim\mathcal{D}^2L_{\rm SA}^4/r_\varphi^4$ and $\kappa^2\sim\mathcal{D}^2L_{\rm SA}^2/r_\varphi^2$, whereas the correction term in (104) is $\sim\mathcal{D}^2L_{\rm SA}^2/r_\varphi^2$. Hence, it can originate only from the term due to κ^2 in (108). The latter is obviously associated with the azimuthal shift, see (98). Alternatively, the correction term in (104) can be obtained if we expand the expression for $W'_{\rm A}(\eta)$ in (98) near the maximum of the peak using the Taylor formula:

$$W'_{\rm A}(\eta)\approx N\,\mathrm{sinc}\,\frac{w(\eta+A_1)N}{2}\approx N\Big(1-\frac{1}{6}\Big(\frac{w(\eta+A_1)N}{2}\Big)^2\Big),$$

then substitute $\eta=0$ and use $\langle A_1^2\rangle$ from (94). Thus, we can associate case B and the corresponding asymptotics with the random azimuthal shift of the image due to a random azimuthal gradient of the electron number density.

In contrast to (103), formula (106) pertains to the highest point of the peak of $W'_{\rm A}(\eta)$ regardless of the shift. We have found that formula (106) yields the same result as (105), which is built upon (100). The latter is equivalent to setting $\kappa=0$ in (108). Similarly to the case B, formulae (105)–(106) are insensitive to the common phase shift. Hence, the asymptotics incorporating the expected value of QPE developed in the case C is appropriate for predicting the average decrease of the peak height for an individual image.

Another way of comparing (103)–(104) against (105)–(106) is to say that the former evaluate the maximum of an average, while the latter evaluate the average of the maxima. Indeed, a given realization of the random function $W'_{\rm A}(\eta)$ reaches its maximum near $\eta=-A_1$, where A_1 is a random zero-mean variable, see (90). Formulae (105)–(106) involve the average of the values taken at this random argument, *i.e.*, $\langle|W'_{\rm A}(-A_1)|^2\rangle$. The latter average is deterministic. At the same time, the average of the squared GAF $\langle|W'_{\rm A}(\eta)|^2\rangle$, which is also a deterministic function, peaks at $\eta=0$, see [7], and formula (103) refers to the height of this peak, *i.e.*, $\langle|W'_{\rm A}(0)|^2\rangle$. However, changing the order in which averaging and taking the maximum are done changes the result, because taking the maximum is not a linear operation.

Although these differences of the asymptotics expressions as $\mathcal{D} \to 0$ may seem insignificant, especially as $L_{\rm SA}/r_\varphi \ll 1$, the above analysis helps in understanding the effects at large values of $\mathcal{D}$. Starting with the case A and taking again the limit $r_\varphi \to \infty$ where $f_{mn} \equiv 1$, we notice that the intensity image is undistorted regardless of the value of $\mathcal{D}$. Formula (67) is also valid for large $\mathcal{D}$ and yields an exponentially small value of the statistical average $\langle W'_{\rm A}(0)\rangle$ once $\mathcal{D} \gtrsim 1$: $\langle W'_{\rm A}(0)\rangle/N = e^{-\mathcal{D}^2} \ll 1$. However, as was already mentioned, this is a result of averaging of the common phase factor (107) over the ensemble of images. The latter operation makes little sense for most practical purposes. Another way toward understanding this effect is to notice that the complex random variable $W'_{\rm A}(0)/N$ has its values on the unit circle. A small value of $\langle W'_{\rm A}(0)/N\rangle$ observed at $\mathcal{D} \gtrsim 1$ tells us is that the complex angle of $W'_{\rm A}(0)$, which is equal to the remainder $((-wA_0) \mod 2\pi)$, approaches a uniform distribution on $[0, 2\pi)$ if $\mathcal{D} \gtrsim 1$. The latter is true because $\langle (wA_0)^2\rangle \approx w^2\langle \zeta_0^2\rangle = 2\mathcal{D}^2$, see (52) and (94)–(95).

Turning to the case B for $\mathcal{D}L_{\rm SA}/r_\varphi \gtrsim 1$, we note that the first approximate equality in (103) will result in a substantially lower value of the average image intensity at the true scatterer location $y_1 = z_1$ compared to the unperturbed case $W_{\rm A} = N\,\mathrm{sinc}(w\eta N/2)$, see (64). As we have established that this case describes the effect of azimuthal shift, the correct way to interpret this drop of image intensity is to realize that when $\mathcal{D}L_{\rm SA}/r_\varphi \gtrsim 1$, the average magnitude of the shift is big enough for the true scatterer location to fall beyond the main lobe of the peak, as shown by (99).

Finally, we have shown that the case C is free from the effects of argument or phase shift of $W'_{\rm A}(\eta)$. Even for $\mathcal{D} \gg 1$, we can obtain images with low level of blurring as long as $\mathcal{D}L_{\rm SA}^2/r_\varphi^2 \ll 1$. It is only if the latter condition is violated, *i.e.*, the QPE is expected to be large, that we expect to see significant deterioration of the main lobe of $W'_{\rm A}(\eta)$ manifested by a significant decrease of the peak amplitude.

Let us now directly analyze the effects at the edge of the main lobe of the GAF, *i.e.*, at $\eta = -A_1 \pm 2\pi/(wN)$, see (98). As suggested by formula (26) and the subsequent discussion, the extent of blurring, along with the decrease of the peak amplitude, are characterized by the value of $W'_{\rm A}$ precisely at this location. Evaluating the second moment of $W'_{\rm A}$ directly by means of formula (62) with A_1 given by (88) (similarly to (106)) or, alternatively, using $\langle \phi_\zeta^2\rangle = \langle (wA_2N^2/4)^2\rangle$ in the expression (26) for $\mathcal{W}(\pi,\phi)$, we arrive at one and the same result:

$$\frac{\sqrt{\langle \left|W'_{\rm A}(-A_1 + 2\pi/(wN))\right|^2\rangle}}{N} = \frac{\sqrt{3Q}}{\pi^2}\mathcal{D}\frac{L_{\rm SA}^2}{r_\varphi^2}. \tag{109}$$

Note that if the azimuthal shift were ignored, *i.e.*, $W'_{\rm A}$ were evaluated at $\eta = \pm 2\pi/(wN)$, then the right-hand side of equation (109) would appear $\sim \mathcal{D}L_{\rm SA}/r_\varphi$, *i.e.*, $r_\varphi/L_{\rm SA} \gg 1$ times bigger.

To summarize, the case of large-scale turbulence, $L_{\rm SA} \ll r_\varphi$, requires a different approach compared to the small-scale case of Section 4.3. Namely, the use of $\delta W = W' - W$ in the capacity of the distance (57) as done in (59) or (60) no longer proves helpful for characterizing the image distortions. A more adequate approach is to quantify the distortions by the expected values of the azimuthal shift, see (99), and blurring of the main lobe, see (105), (106), and (109).

4.5 Error Due to Factorization and the Effect of Turbulence on Imaging in Range

Let us consider the second component of $\delta W = W' - W$ as defined in (61):

$$\delta W_2 = (W' - W'_{(\mathrm{R}\Sigma)}) - (W - W_{(\mathrm{R}\Sigma)}) = \delta W_{2a} - \delta W_{2b}.$$

The terms δW_{2a} and δW_{2b} on the right-hand side of the previous equality represent the factorization error of the stochastic and deterministic GAF, respectively. The deterministic term δW_{2b} was studied in Section 2.3. Similarly to the deterministic analysis, it is possible to use the the Taylor formula

$$\mathrm{sinc}(\xi + \eta n - \zeta_n) \approx \mathrm{sinc}\,\xi + \mathrm{sinc}'\,\xi \cdot (\eta n - \zeta_n)$$

to estimate the difference between the stochastic GAF (53) and its approximate factorized representation (56):

$$\begin{aligned}\delta W_{2a} &= W'(\xi,\eta) - W'_{(\mathrm{R}\Sigma)}(\xi,\eta)\\ &= \tau e^{-iw\xi}\sum_n e^{-iw(\eta n+\zeta_n)}(\,\mathrm{sinc}(\xi + \eta n - \zeta_n) - \mathrm{sinc}(\xi)) \approx \tau e^{-iw\xi}\,\mathrm{sinc}'(\xi)\sum_n e^{-iw(\eta n+\zeta_n)}(\eta n - \zeta_n).\end{aligned}$$

For the variance of δW_2, we have, similarly to (70):

$$\sigma^2_{\delta W_2} = \sigma^2_{\delta W_{2a}} = \left\langle |\delta W_{2a} - \langle \delta W_{2a} \rangle|^2 \right\rangle = \tau^2 (\operatorname{sinc}' \xi)^2 \sum_{m,n} C_{mn},$$

where the covariance matrix is

$$C_{mn} = \left\langle \left[e^{-iw(\eta m + \zeta_m)} (\eta m - \zeta_m) - e^{-\mathcal{D}^2} e^{-iw\eta m} \Big(\eta m + i \frac{2\mathcal{D}^2}{w} \Big) \right] \cdot \left[e^{iw(\eta n + \zeta_n)} (\eta n - \zeta_n) - e^{-\mathcal{D}^2} e^{iw\eta n} \Big(\eta n - i \frac{2\mathcal{D}^2}{w} \Big) \right] \right\rangle. \quad (110)$$

From the definitions of η and ζ_n in (51), one can see that compared to the azimuthal covariance matrix given by (71), the terms in (110) are about $w^2 \gg 1$ smaller (see (52)). Then, the same relation may exist between the variances of δW_1 and δW_2: $\sigma^2_{\delta W_2} \ll \sigma^2_{\delta W_1}$. As the term δW_1 pertains exclusively to azimuth, see formulae (61) and (65), the previous inequality sometimes leads to an assumption that the ionospheric turbulence does not affect the SAR performance in range at all, see, *e.g.*, [7].

In [1, Section 4.4], the inequality $\sigma^2_{\delta W_2} \ll \sigma^2_{\delta W_1}$ has been shown true in the case of $\mathcal{D} \ll 1$ and $r_\varphi \ll L_{\mathrm{SA}}$. The case $r_\varphi \ll L_{\mathrm{SA}}$ with $\mathcal{D} \gg 1$ is of no practical interest because image distortions are large due to azimuthal effects, see Section 4.3.3. The remaining case of $L_{\mathrm{SA}} \ll r_\varphi$ can be analyzed using its similarity to that of a quasi-homogeneous ionosphere, see Section 3.2.2. In order to adapt formula (34) to the stochastic case, we make the following substitution:

$$\frac{1}{L_Q} \tilde{\omega}^2_{\mathrm{pe}} \longrightarrow \frac{\partial}{\partial x_1} \omega^2_{\mathrm{pe},\mu}(\boldsymbol{x}, \boldsymbol{z}),$$

where $\omega^2_{\mathrm{pe},\mu}$ is the perturbation of the effective plasma frequency responsible for the perturbation of the eikonal, see (38):

$$\omega^2_{\mathrm{pe},\mu}(\boldsymbol{x}, \boldsymbol{z}) = \frac{4\pi e^2}{m_{\mathrm{e}}} \frac{1}{R_{\boldsymbol{z}}} \int_0^{R_{\boldsymbol{z}}} \mu(\boldsymbol{x}(r))\, dr \quad \Rightarrow \quad \varphi(\boldsymbol{x}^n, \boldsymbol{z}) = R \frac{\omega^2_{\mathrm{pe},\mu}(\boldsymbol{x}, \boldsymbol{z})}{\omega_0^2}.$$

Expressing φ_n via ζ_n with the help of (51) and using (87) and (92) to calculate $d\zeta/dx_1$, we have:

$$\frac{1}{L_Q} \tilde{\omega}^2_{\mathrm{pe}} \longrightarrow \frac{\omega_0^2}{R} \frac{2c}{B} \frac{N}{L_{\mathrm{SA}}} A_1.$$

Then, using the estimate for $\langle A_1^2 \rangle$ given by (94), we obtain from (34):

$$\left\langle \left| \frac{W' - W'_{(\mathrm{R}\Sigma)}}{\max |W_{(\mathrm{R}\Sigma)}|} \right|^2 \right\rangle \sim 2^{-6} \langle A_1^2 \rangle N^2 = \left(\frac{\sqrt{K}}{4} \frac{\mathcal{D}}{w} \frac{L_{\mathrm{SA}}}{r_\varphi} \right)^2.$$

This distortion turns out to be smaller than the smallest of the azimuthal distortions, *i.e.*, the one given by (105). The ratio of the former to the latter is $\frac{1}{w} \frac{r_\varphi}{L_{\mathrm{SA}}} \ll 1$. Hence, the contribution of the range effects into the overall image distortions due to ionospheric turbulence can be disregarded in the large-scale case as well.

5 DISCUSSION

We have studied the effect of randomness on transionospheric SAR imaging in two opposite limiting cases: the small-scale turbulence where the correlation radius of the eikonal (considered of the same order of magnitude as that of the medium) is much shorter than the length of the synthetic aperture, as well as the opposite, *i.e.*, large-scale, case, where the correlation radius of the eikonal is much longer than the synthetic aperture. While statistical approach has been employed to describe the turbulence, we were interested in quantifying the distortions in an individual image.

In the small-scale case, $r_\varphi \ll L_{\mathrm{SA}}$, the stochasticity manifests itself through interactions between the "clusters" of correlated phases in the azimuthal sum (62), as explained in Section 4.3.2, see (81) and the subsequent discussion. On the contrary, in the large-scale case, $L_{\mathrm{SA}} \ll r_\varphi$, there is only a "small amount of stochasticity" in the collection of phases that yields an individual image via the azimuthal sum (62). The randomness can rather be observed on the image-to-image basis, *i.e.*, for the statistical ensemble of images. Namely, their azimuthal and phase shifts (99) and

(107), as well as the degree of their blurring (109), are random functions that can be characterized in terms of the corresponding moments. As the analysis in Section 4.4 shows, the requirement that the image blurring be small is weaker than the requirement that the azimuthal shift be small, which, in turn, is weaker than the requirement that the phase shift be small, all in terms of the respective expected values. Accordingly, in the case of $r_\varphi/L_{\rm SA} \gg 1$, if the intensity of the turbulence satisfies $r_\varphi/L_{\rm SA} \ll \mathcal{D} \ll (r_\varphi/L_{\rm SA})^2$, then the azimuthal shift is likely to be large compared to the azimuthal resolution yet the image blurring is expected to remain low.

The analysis of the large-scale case in Section 4.4 can also offer some insight into the case of large eikonal fluctuations in the small-scale regime, see Section 4.3.3. In particular, take formula (85) for r_W derived from the expression for the correlation between the signals $e^{-iw\zeta(x_1)}$. We see that the powers of $\mathcal{D}$ and $L_{\rm SA}/r_\varphi$ in this expression are the same, similarly to formula (99) that gives the magnitude of the azimuthal shift relative to the azimuthal resolution (see also case B in Section 4.4). We can interpret this observation as an indication that the mechanism of distortions described by (85)–(86) is the random azimuthal shifts of "sub-images" that originate from "sub-apertures" of length $r_W = r_\varphi/\mathcal{D}$, such that the decorrelation between the sub-images is due to the difference between their azimuthal shifts. At the same time, in the case of a single (sub-)image, the correlation length for the signals may be determined from the criterion of image blurring, *i.e.*, $r'_W = r_\varphi/\sqrt{\mathcal{D}} \gg r_W$, see (102). More work is needed to explore the possibilities of building a new autofocus algorithm (see [13] for an overview) and/or improve performance of the coherent interferometric (CINT) imaging, see [14], that would take advantage of these observations.

ACKNOWLEDGEMENT

The material presented in this paper is based upon work supported by the US Air Force Office of Scientific Research (AFOSR) under awards number FA9550-14-1-0218 and FA9550-17-1-0230.

REFERENCES

[1] M. Gilman, E. Smith, and S. Tsynkov, *Transionospheric Synthetic Aperture Imaging* (Applied and Numerical Harmonic Analysis. Birkhäuser/Springer, Cham, Switzerland, 2017).

[2] A. S. Monin and A. M. Yaglom, *Statistical Fluid Mechanics: Mechanics of Turbulence* Vol. 1 (The MIT Press, Cambridge, MA, 1971).

[3] S. M. Rytov, Yu. A. Kravtsov, and V. I. Tatarskii, *Principles of Statistical Radiophysics. Vol. 4. Wave Propagation Through Random Media* (Springer-Verlag, Berlin, 1989); Translated from the second Russian edition by Alexander P. Repyev.

[4] J.-P. Fouque, J. Garnier, G. Papanicolaou, and K. Sølna, *Wave Propagation and Time Reversal in Randomly Layered Media*, Vol. 56 of *Stochastic Modelling and Applied Probability* (Springer, New York, 2007).

[5] S. M. Rytov, Yu. A. Kravtsov, and V. I. Tatarskii, *Principles of Statistical Radiophysics. Vol. 3. Elements of Random Fields* (Springer-Verlag, Berlin, 1989); Translated from the second Russian edition by Alexander P. Repyev.

[6] B. V. Gnedenko, *Theory of Probability* 6th edn (Gordon and Breach, Amsterdam, 1997); Translated from Russian.

[7] J. Garnier and K. Sølna (2013) A multiscale approach to synthetic aperture radar in dispersive random media, *Inverse Problems* **29**, 054006, 18p.

[8] R. B. Ash, *Real Analysis and Probability*, Vol. 11 of *Probability and Mathematical Statistics* (Academic Press, New York-London, 1972).

[9] N. A. Armand (2005) On limitation of the resolution of space born synthetic aperture radars caused by the conditions of radio propagation in ionosphere, *Exploration of Earth from Space* **(1)**, 27–38. [in Russian]

[10] W. D. Brown and D. C. Ghiglia (1988) Some methods for reducing propagation-induced phase errors in coherent imaging systems. I. Formalism, *J. Opt. Soc. Am. A – Opt. Image Sci.* **5**(6), 924–941.

[11] C. Oliver and S. Quegan, *Understanding Synthetic Aperture Radar Images* (Artech House Remote Sensing Library, Artech House, Boston, 1998).

[12] J. W. Goodman (1976) Some fundamental properties of speckle, *J. Opt. Soc. Am.* **66**(11), 1145–1150.

[13] Jr. C. V. Jakowatz, D. E. Wahl, P. H. Eichel, D. C. Ghiglia, and P. A. Thompson, *Spotlight-Mode Synthetic Aperture Radar: A Signal Processing Approach* (Springer, 1996).

[14] J. Garnier and K. Sølna (2008) Coherent interferometric imaging for synthetic aperture radar in the presence of noise, *Inverse Problems* **24**(5), 055001, 23p.